Measurement Science and
Technology

PAPER • **OPEN ACCESS**

Continuous approximation of the ZARC element with passive components

To cite this article: Thomas Heil and Andreas Jossen 2021 *Meas. Sci. Technol.* **32** 104011

View the article online for updates and enhancements.

You may also like

- Fluctuations of entropy production in partially masked electric circuits
Kuan-Hsun Chiang, Chia-Wei Chou, Chi-Lun Lee et al.
- Investigation of analog charge multiplexing schemes for SiPM based PET block detectors
Evan Downie, Xin Yang and Hao Peng
- A novel power source for high-precision, highly efficient micro w-EDM
Shun-Tong Chen and Chi-Hung Chen

This content was downloaded from IP address 202.8.112.182 on 19/06/2023 at 11:30

OPEN ACCESS
IOP Publishing
Measurement Science and Technology
Meas. Sci. Technol. **32** (2021) 104011 (20pp)
https://doi.org/10.1088/1361-6501/ac0466

Continuous approximation of the ZARC element with passive components

Thomas Heil* **and Andreas Jossen***

Technical University of Munich (TUM), Institute for Electrical Energy Storage Technology (EES), Arcisstrasse 21, 80333 Munich, Germany

E-mail: thomas.heil@tum.de and andreas.jossen@tum.de

Received 20 January 2021, revised 3 May 2021
Accepted for publication 24 May 2021
Published 6 July 2021

Abstract

The ZARC element is a parallel connection between a constant phase element and an ohmic resistor which describes the charge transfer and the double-layer capacitance at an electrode–electrolyte interface. However, this mathematical object has been determined using measurement data and cannot be derived from physical or chemical processes. In order to understand the dynamics of ZARC and its parameters' influence in frequency and in time domain, we approximate it using fundamental equivalent circuits. Here, we introduce two approaches using RC circuits whose behaviours are well-known. The first method consists of infinitely many serially connected RC circuits which can be uniquely related to ZARC by explicit equations. In contrast, the second uses just three serially connected RC circuits, but adds a minimization problem. Both approaches depend only on three parameters: an ohmic resistance, a capacitance, and a newly defined parameter which is a measure of the modification of the single capacitances. Moreover, we show a decrease of the total capacitance of both impedances for growing deviations from the behavior of an RC circuit. Finally, since the properties of RC circuits are well known in frequency and in time domain, we deduce the behaviours of both methods in the time domain.

Keywords: ZARC element, R/Q element, constant phase element, electrode–electrolyte interface, charge transfer, double-layer capacitance

(Some figures may appear in colour only in the online journal)

1. Introduction

In 1941, Cole and Cole extended Debye's theory [1] to the frequency dependence of the dielectric constant of solids and liquids [2]. After many measurements, they established the influence of the frequency using an exponential damping factor, called α. Debye's theory sets α equal to one, whereas Cole and Cole defined the domain as the interval $[0;1]$; Jonscher restricts the interval to $[0.6;0.95]$ [3]. In addition to the equation:

$$\epsilon^* - \epsilon_\infty = \frac{\epsilon_0 - \epsilon_\infty}{1 + (\mathrm{i}\omega\tau_0)^\alpha}, \tag{1}$$

for the dielectric constant ϵ^*, where ϵ_∞, ε_0, and τ_0 depend on the analysed media, Cole and Cole also gave an equivalent electrical circuit describing the behaviour, which they analysed in the frequency domain. For this purpose, they chose the constant phase element (CPE) introduced by Fricke in [4]. The CPE is an impedance, with a constant phase that is independent of the frequency:

$$Z_{\mathrm{CPE}}(\omega) = \frac{1}{(\mathrm{i}\omega)^\alpha K}, \tag{2}$$

* Authors to whom any correspondence should be addressed.

Original Content from this work may be used under the terms of the Creative Commons Attribution 4.0 licence. Any further distribution of this work must maintain attribution to the author(s) and the title of the work, journal citation and DOI.

where K is a kind of capacitance, with units depending on α. In [2], Cole and Cole also showed an approximation of the measured data for the parallel connection of an ohmic resistance R with the CPE, called the ZARC element or the RQ element, which was a better fit than the parallel connection of an ohmic resistor and a capacitor with resistance R and capacitance C, called an RC circuit. The total impedance of the ZARC element is:

$$Z_{\mathrm{ARC}}(\omega) = \frac{R}{1+(\mathrm{i}\omega)^{\alpha} RK}. \tag{3}$$

According to Fricke [4] and Randles [5], the ZARC element can be interpreted as the charge-transfer reaction occurring, for example, in batteries, supercapacitors, and fuel cells [6].

Cole and Cole were not the only ones to discover the so-called CPE behaviour in their measurement data. There are further electrochemical, physical, and biological systems in which the same CPE characteristics have been detected [7–13]. According to these reports, the origin of the CPE behaviour is a distribution of reactivity, faradaic reactions, or the distribution of time constants as a consequence of geometrical and electrical inhomogeneities. Brug *et al* confirmed the thesis of the distribution of time constants in [6]; moreover, they assumed a constant ohmic resistance and distributed capacitances. There have been various attempts to approximate the CPE using RC networks, which started by approximating the impedance using rational functions or continued fractions [14–18]. Finally, Buller [19, 20, pp. 77 ff.], Farmann *et al* [21] and Handschuh [22, pp. 143 ff.] supplied some optimized algorithms to approximate the ZARC element using three or five RC circuits in the frequency domain. Buller and Farmann *et al* presented their results as a lookup table for certain values of α. However, there has been no investigation of this behaviour in the time domain.

The ZARC element describes the measurement data of electrochemical systems in the frequency domain very well [2, 7]. However, there is also great interest in analysing these systems in the time domain. For example, battery management systems that monitor single cells and battery packs work in the time domain [23]. Besides, many algorithms for state estimation need time-dependent models [24–26]. Hence, it is necessary to know the behaviour of the ZARC element in the time domain. Using the Mittag–Leffler function [27], the time behaviour of the ZARC element can be computed. However, the result is an alternating series with non-integer exponents of time. For this reason, the physical interpretation, in the sense of dealing with dynamic systems with unique time constants, is unclear.

In this paper, we introduce two approaches to the approximation of the ZARC element using passive components that have fixed time constants. For this purpose, we use the geometric properties of ZARC in a Nyquist diagram to construct two impedances on the basis of serially connected RC circuits. The first impedance, called ZAPP from Z for impedance and APP for approximation of the ZARC element, follows the ansatz of Brug *et al* described in [6] and uses infinitely many identical ohmic resistances with varying capacitances. In this case, the parameters of ZARC can be expressed as functions of the ZAPP parameters. The impedance Z_{3RC} of the second approximation consists of three RC circuits with varying ohmic resistances and varying capacitances. Compared to ZAPP, the additional degree of freedom, however, requires a minimization algorithm to relate the three parameters of Z_{3RC} to the parameters of ZARC. In both cases, we also derive an explicit distribution of the time constants, and show the behaviours of the approximations and the ZARC element in the time domain.

For reasons of clarity and comprehensibility, we present lengthy derivations in the appendices.

2. Approximation of the ZARC element

2.1. Mathematical properties of the ZARC element

As mentioned above, the ZARC element has a purely empirical origin. In order to show that it is physical, we first have to prove that it satisfies the general conditions of linearity, invariance in time, finiteness, stability, and causality. According to Urquidi-Macdonald and Macdonald, [28–30], the properties are fulfilled iff the Kramers–Kronig relation is satisfied. However, this is a consequence of all analytic functions. So, it is sufficient to prove that ZARC is an analytic function. From complex analysis, we know that a function is analytic if and only if the Cauchy-Riemann equations are applicable. In order to show this, we start with a function $f(x+iy) = (x+iy)^{\alpha}$ satisfying the Cauchy–Riemann equations:

$$\begin{aligned}\frac{\partial \mathrm{Re}\left[f(x+\mathrm{i}y)\right]}{\partial x} &= \frac{\alpha}{2}\left((x+\mathrm{i}y)^{\alpha-1} + (x-\mathrm{i}y)^{\alpha-1}\right)\\ &= \frac{\partial \mathrm{Im}\left[f(x+\mathrm{i}y)\right]}{\partial y},\end{aligned} \tag{4}$$

$$\begin{aligned}\frac{\partial \mathrm{Re}\left[f(x+\mathrm{i}y)\right]}{\partial y} &= \frac{i\alpha}{2}\left((x+\mathrm{i}y)^{\alpha-1} - (x-\mathrm{i}y)^{\alpha-1}\right)\\ &= -\frac{\partial \mathrm{Im}\left[f(x+\mathrm{i}y)\right]}{\partial x}.\end{aligned} \tag{5}$$

Since all linear combinations of analytic functions are analytic, and at each maximal domain, the inverse of an analytic function is also analytic, so is the function $1/1+(x+iy)^{\alpha}$ and hence ZARC is also analytic [31]. Therefore, the ZARC element satisfies the Kramers–Kronig relation. In particular, the proof includes the case $\alpha = 1$, which represents an RC circuit.

Moreover, we proceed with some geometric properties of the ZARC element. Cole and Cole correctly explained in [2] that ZARC is an arc in the first quadrant of the Nyquist diagram, hence the name 'Z-ARC'! In appendix A, we prove that the impedance corresponds to the equation for a circle:

$$\begin{aligned}&\left(\mathrm{Re}\left[Z_{\mathrm{ARC}}(\omega)\right] - \frac{R}{2}\right)^2 + \left(\mathrm{Im}\left[Z_{\mathrm{ARC}}(\omega)\right] - \frac{R}{2\,\tan\left(\frac{\alpha}{2}\pi\right)}\right)^2\\ &= \left(\frac{R}{2\,\sin\left(\frac{\alpha}{2}\pi\right)}\right)^2,\end{aligned} \tag{6}$$

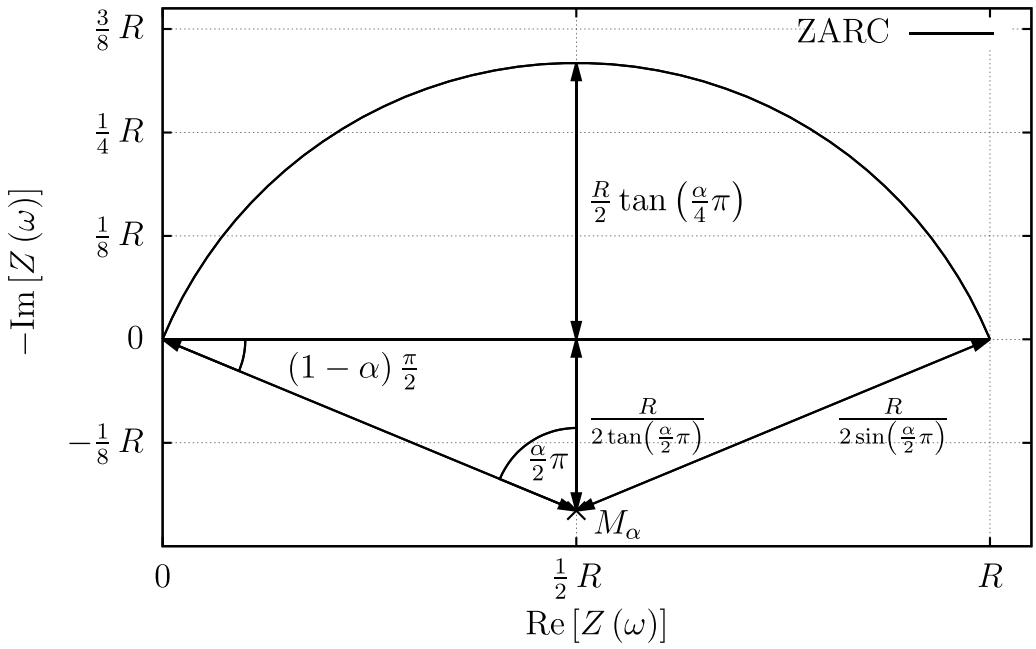

Figure 1. Geometry of ZARC with $\alpha = 0.75$.

with

$$\mathrm{Re}\left[Z_{\mathrm{ARC}}\left(\omega\right)\right] = \frac{1 + \left(\omega^{\alpha} RK\right)\cos\left(\frac{\alpha}{2}\pi\right)}{1 + 2\ \left(\omega^{\alpha} RK\right)\cos\left(\frac{\alpha}{2}\pi\right) + \left(\omega^{\alpha} RK\right)^{2}} R \quad (7)$$

$$\mathrm{Im}\left[Z_{\mathrm{ARC}}\left(\omega\right)\right] = \frac{-\left(\omega^{\alpha} RK\right)\sin\left(\frac{\alpha}{2}\pi\right)}{1 + 2\ \left(\omega^{\alpha} RK\right)\cos\left(\frac{\alpha}{2}\pi\right) + \left(\omega^{\alpha} RK\right)^{2}} R. \quad (8)$$

The centre of the arc is at $M_\alpha = \left(R/2; R/2\ \tan\left(\frac{\alpha}{2}\pi\right)\right)$ and the radius is $R/2\ \sin\left(\frac{\alpha}{2}\pi\right)$. The geometric function of α represents a shift of the centre in the Im direction and an adaption of the radius. There is no depressed semicircle at all. Figure 1 shows more distances and angles that describe ZARC in a Nyquist diagram. Moreover, the impedance moves counterclockwise from $Z_{\mathrm{ARC}}\left(\omega = 0\ \right) = R$ to $Z_{\mathrm{ARC}}\left(\omega \to \infty\right) = 0$. Additionally, the local extrema of the imaginary part is at $\omega^{\alpha} RK = 1$ and takes the value $-R/2 \cdot \tan\left(\alpha/4\pi\right)$. Moreover, the former condition gives a notion of the parameter K, which is the velocity at which the arc is passed. The larger the value of K, the faster the impedance moves in the direction of the coordinate origin with respect to ω.

2.2. Behaviour of the ZARC element in the time domain

According to Heaviside's definition of impedance [32, pp. 370 ff.] [33, pp. 61 ff.], the voltage response of a system with impedance $Z(z)$ to a current step with amplitude I is:

$$U(t) = I \int_0^t \mathcal{L}^{-1}\left\{Z(z)\right\}(\tilde{t})\,\mathrm{d}\tilde{t}. \quad (9)$$

Here, $\mathcal{L}^{-1}$ is the inverse Laplace transformation and $z = \sigma + \mathrm{i}\omega$. In the following, we set $\sigma = 0$, where ω is the non-negative angular frequency, as above. Using the Mittag–Leffler function, the inverse Laplace transformation of the ZARC element is:

$$\mathcal{L}^{-1}\left\{Z_{\mathrm{ARC}}\left(z\right)\right\}\left(\mathrm{t}\right) = \frac{1}{K} t^{\alpha-1} \sum_{n=0}^{\infty} \frac{1}{\Gamma\left(\left(n+1\right)\alpha\right)} \left(-\frac{t^{\alpha}}{RK}\right)^{n}, \quad (10)$$

hence, the voltage response to a current step in the ZARC element is:

$$U_{\mathrm{ARC}}\left(t\right) = RI \sum_{n=0}^{\infty} \frac{(-1)^{n} t^{(n+1)\alpha}}{(RK)^{n+1}\,\Gamma\left(\left(n+1\right)\alpha + 1\ \right)}, \quad (11)$$

with the gamma function $\Gamma\left(x\right)$. The detailed computation is given in appendix B. In general, the Mittag–Leffler function is used to describe anomalous relaxation, mass transport, and diffusion processes with fractional kinetic equations that differ from the standard Debye relaxation [34, pp. 3 ff., pp. 259 ff.] and [35–37]. Due to the choice of α, the Mittag–Leffler function represents an exponential function or a hyperbolic sinus of the square root, divided by the square root [38, pp. 18 ff.].

2.3. Symmetric serial connection of two RC circuits

In the following, we introduce a new method that creates a symmetric impedance in the Nyquist diagram out of two serially connected RC circuits. The symmetry is mirror-symmetric to a straight line through $(R/2; 0\ )$ and parallel to the imaginary-part axis. For this purpose, we use the properties of the ZARC element from above and the properties of an RC circuit with an ohmic resistance R and a capacitance C. Moreover, for an impedance $Z(\omega)$, we define the angle φ at

the vertex $(R/2;0)$ enclosed by the ray through $(R/2;0)$ and $Z(\omega)$ and the real-part axis,

$$\tan(\varphi) = \frac{-\mathrm{Im}[Z(\omega)]}{\mathrm{Re}[Z(\omega)] - \frac{R}{2}}. \tag{12}$$

This equation relates the non-negative frequency $\omega \in \mathbb{R}_0^+$ to the angle $\varphi \in [0, \pi]$. Therefore, the impedance, generally expressed as a function of the frequency ω, can be expressed as a function of φ, $Z(\omega) = Z(\omega(\varphi)) = Z(\varphi)$. Thus, for a simple RC circuit with impedance:

$$Z_{RC}(\omega) = \frac{R}{1 + \mathrm{i}\omega RC}, \tag{13}$$

the following equations hold true:

$$\tan\left(\frac{\varphi}{2}\right) = \omega RC \tag{14}$$

$$Z_{RC}(\varphi) = \frac{R}{2}(1 + \cos(\varphi)) - \mathrm{i}\frac{R}{2}\sin(\varphi) = \frac{R}{2}\left(1 + \mathrm{e}^{-\mathrm{i}\varphi}\right). \tag{15}$$

It is obvious that $Z_{RC}(\varphi)$ is correct, since it is just the geometric expression of the impedance in the Nyquist diagram. In appendix C, we present a more detailed computation of (14) and (15).

Using the following theorem, we show that for the serial connection of two RC circuits to be mirror-symmetric only requires identical ohmic resistances. Moreover, the mirror-symmetric property is independent of the choice of the two capacitances. Please note that the detailed derivations can be found in appendix D.

Theorem 1. *Let $Z_{R_+C_+}(\omega)$ and $Z_{R_-C_-}(\omega)$ be the impedances of two RC circuits with the parameters R_+, C_+ and R_-, C_-, respectively. Let the two ohmic resistances be identical, i.e. $R_+ = R_- = R/2$, then the serial connection of the impedances $Z_{2RC}(\omega) = Z_{R_+C_+}(\omega) + Z_{R_+C_+}(\omega)$ is mirror-symmetric in the Nyquist diagram, i.e. $Z_{2RC}(\varphi) + \overline{Z_{2RC}(\pi - \varphi)} = R$, with φ as defined in (12). The bar denotes the complex conjugate of the number.*

Proof. Let φ_+ and φ_- be the angles of the single RC circuits to the same frequency ω according to (14)

$$\tan\left(\frac{\varphi_\pm}{2}\right) = \omega R_\pm C_\pm, \tag{16}$$

where the capacitances C_+ and C_- are arbitrary. The total impedance is due to (15):

$$Z_{2\,\mathrm{RC}}(\varphi_+, \varphi_-) = \frac{R}{2}\left(1 + \cos\left(\frac{\varphi_+ - \varphi_-}{2}\right) \cdot \mathrm{e}^{-\mathrm{i}\frac{\varphi_+ + \varphi_-}{2}}\right), \tag{17}$$

and φ, as defined in (12), is:

$$\begin{aligned}\tan(\varphi) &= \tan\left(\frac{\varphi_+ + \varphi_-}{2}\right) = \frac{\tan\left(\frac{\varphi_+}{2}\right) + \tan\left(\frac{\varphi_-}{2}\right)}{1 - \tan\left(\frac{\varphi_+}{2}\right)\tan\left(\frac{\varphi_-}{2}\right)} \\ &= \frac{(\omega R_+ C_+) + (\omega R_- C_-)}{1 - (\omega R_+ C_+)(\omega R_- C_-)}.\end{aligned} \tag{18}$$

Let $\tilde{\varphi} = \pi - \varphi = \tilde{\varphi}_+ + \tilde{\varphi}_-/2$ be the angle at the mirror-symmetric point of $Z_{2RC}(\omega)$, denoted by $Z_{2RC}(\tilde{\omega})$, then the angles $\tilde{\varphi}_\pm$ of each RC circuit can be related to $\varphi_\mp$ through:

$$\tilde{\varphi}_\pm = \pi - \varphi_\mp. \tag{19}$$

This holds true due to the comparison of the single terms and the usage of the trigonometric relation of the tangent. Further details of the explicit derivation are given in appendix D. Substituting this into (17) leads to:

$$\begin{aligned}&Z_{2RC}(\varphi) + \overline{Z_{2RC}(\pi - \varphi)} \\ &\quad = Z_{2\,\mathrm{RC}}(\varphi_+, \varphi_-) + \overline{Z_{2\,\mathrm{RC}}(\tilde{\varphi}_+, \tilde{\varphi}_-)} \\ &\quad = Z_{2\,\mathrm{RC}}(\varphi_+, \varphi_-) + \overline{Z_{2\,\mathrm{RC}}(\pi - \varphi_-, \pi - \varphi_+)} \\ &\quad = \frac{R}{2}\left(1 + \cos\left(\frac{\varphi_+ - \varphi_-}{2}\right) \cdot \mathrm{e}^{-\mathrm{i}\frac{\varphi_+ + \varphi_-}{2}}\right) \\ &\qquad + \frac{R}{2}\left(1 - \cos\left(\frac{\varphi_+ - \varphi_-}{2}\right) \cdot \mathrm{e}^{-\mathrm{i}\frac{\varphi_+ + \varphi_-}{2}}\right) = R\end{aligned} \tag{20}$$

which proves the mirror symmetry.

□

We continue with the two RC circuits and their serial connection as in the theorem above. One question remains unanswered: how does the choice of C_+ and C_- affect the impedance graph of the serial connection in the Nyquist diagram? From (16) and (17), we know that if the two capacitances are approximately equal to each other, then it is also true that the angles $\varphi_\pm$ almost coincide. Therefore, the cosine in (17) is almost equal to one, and $Z_{2RC}(\omega)$ behaves like a single RC circuit with an ohmic resistance R and a capacitance $C_+ \approx C_-$. However, if the capacitances differ widely, e.g. $C_+ \gg C_-$, the angles are also distinguished, and consequently, the cosine in (17) is less than 1. In particular, this can be seen for frequencies in the range of $\omega \approx 1/R_+\sqrt{C_+C_-}$. In this case,

$$\begin{aligned}\tan\left(\frac{\varphi_+}{2}\right) &= \sqrt{\frac{C_+}{C_-}} = \frac{1}{\sqrt{\frac{C_-}{C_+}}} = \frac{1}{\tan\left(\frac{\varphi_+}{2}\right)} \\ &= \tan\left(\frac{\pi}{2} - \frac{\varphi_-}{2}\right) \gg 1,\end{aligned} \tag{21}$$

holds true and hence $\varphi_+ = \pi - \varphi_-$. Furthermore, since

$$\tan\left(\frac{\varphi_-}{2}\right) = \sqrt{\frac{C_-}{C_+}} \ll 1, \tag{22}$$

it is also the case that $\varphi_- \ll \pi/2$, thus, the difference $\varphi_+ - \varphi_- = \pi - 2\varphi_-$ is close to π. Consequently, the cosine in

(17) goes to zero and the graph of the total impedance reaches a peak in the direction of the positive imaginary-part axis. Moreover, since $\varphi = \varphi_+ + \varphi_-/2 = \pi/2$ at $\omega = 1/R_+\sqrt{C_+C_-}$, the impedance lies on the mirror axis. As a result, the total impedance always has a local extremum at the point $(R/2; \sqrt{C_+C_-}R/(C_+ + C_-))$. In summary, the more the two capacitances differ from each other, the more the single RC circuits appear in the Nyquist plot of the total impedance.

Furthermore, we insert a reference capacitance called C that scales the total impedance and choose $\omega = 1/RC$ to be the frequency of the local extrema of $Z_{2RC}(\omega)$ in the Nyquist diagram at $\mathrm{Re}[Z_{2RC}(\omega)] = R/2$. Therefore, $\varphi = (\varphi_+ + \varphi_-)/2 = \pi/2$ holds true at that frequency. In order to regulate the local extrema of the total impedance $Z_{2RC}(\omega)$ in a more convenient way, we introduce a measure β for the deviation of the two capacitances from each other. Accordingly, we define the difference of the angles as follows:

$$\varphi_+ - \varphi_- = 2\,\beta, \tag{23}$$

and hence

$$\varphi_\pm = \frac{\pi}{2} \pm \beta \tag{24}$$

at the frequency $\omega = 1/RC$, and as a consequence of (14), we determine the single capacitances according to:

$$C_\pm = \frac{1}{\omega R_\pm}\tan\left(\frac{\varphi_\pm}{2}\right) = 2C\tan\left(\frac{\pi}{4} \pm \frac{\beta}{2}\right), \tag{25}$$

depending on β. Therefore, the angle β modifies the capacitances and can be interpreted as a measure of the deviation of the two capacitances. Since $\varphi_\pm \in [0,\pi]$, the domain of β is restricted to the interval $[0,\pi/2)$. The choice $\beta = \pi/2$ is excluded, since it would lead to the unreasonable case of $C_+ = +\infty$ (short circuit) and $C_- = 0$ (open circuit). Furthermore, the total impedance of the two serially connected RC circuits with identical ohmic resistances and $C_\pm$ as defined in (25) is:

$$\begin{aligned} Z_{2RC}(\omega) &= \frac{R_+}{1+\mathrm{i}\omega R_+C_+} + \frac{R_-}{1+\mathrm{i}\omega R_-C_-} \\ &= \frac{\cos^2(\beta)\left(1-(\omega RC)^2\right) + 2\,(\omega RC)^2}{\cos^2(\beta)\left(1-(\omega RC)^2\right)^2 + 4\,(\omega RC)^2}R \\ &\quad - \mathrm{i}\frac{\cos(\beta)(\omega RC)\left(1+(\omega RC)^2\right)}{\cos^2(\beta)\left(1-(\omega RC)^2\right)^2 + 4\,(\omega RC)^2}R, \end{aligned} \tag{26}$$

and the angle φ is given by:

$$\tan(\varphi) = \frac{2\,(\omega RC)}{1-(\omega RC)^2}\frac{1}{\cos(\beta)}, \tag{27}$$

at the vertex $(R/2;0)$. The computations of both the equations above are shown in appendix D. Figure 2(a) shows how the total impedance is composed of the individual RC circuits, whereas 2(b) represents the Nyquist plots for varying β. This confirms that the more the capacitances differ from each other, i.e., the bigger β is, the more the local extrema are stressed in the middle.

Additionally, we derive the relationship between two frequencies, ω and $\tilde{\omega}$, belonging to mirror-symmetric points on Z_{2RC} in the Nyquist diagram. Let φ and $\tilde{\varphi} = \pi - \varphi$ again be the angles corresponding to $Z_{2RC}(\omega)$ and to $Z_{2RC}(\tilde{\omega})$, respectively. The frequencies fulfil the condition $(\omega RC)(\tilde{\omega}RC) = 1$, since

$$\begin{aligned} \tan(\tilde{\varphi}) = \tan(\pi-\varphi) = -\tan(\varphi) &= \frac{2\,\frac{1}{(\omega RC)}}{1-\frac{1}{(\omega RC)^2}}\frac{1}{\cos(\beta)} \\ &= \frac{2\,(\tilde{\omega}RC)}{1-(\tilde{\omega}RC)^2}\frac{1}{\cos(\beta)} \end{aligned} \tag{28}$$

holds true.

2.4. Approximation with infinitely many RC circuits

2.4.1. Approximation in the frequency domain. According to figure 2 (b), the Nyquist plots of two serially connected RC circuits are not uniformly depressed but rather depressed at a specific point. In order to create a uniform depression, we connect $2N$ pairs of RC circuits as described above with one special RC circuit. They fulfil the following conditions:

(a) The sum over all identical ohmic resistances is R, i.e. $\sum_{n=-N}^{N} R_n = R$, where $R_n = R_m$, for $-N \leqslant n,m \leqslant N$.
(b) For convenience, we choose the real part of the total impedance of the serial connection at the frequency $\omega = \frac{1}{RC}$ to be $\mathrm{Re}\left[Z_{\mathrm{total}}\left(\omega = \frac{1}{RC}\right)\right] = \mathrm{Re}\left[Z_{\mathrm{total}}\left(\varphi = \frac{\pi}{2}\right)\right] = \frac{R}{2}$.

The pairwise capacitances are chosen in such a way that the deviation of the angle φ from $\pi/2$ at $\omega = 1/RC$ is reduced in equal steps from β to zero. The equal steps ensure a uniform curvature of the total impedance in the Nyquist diagram. Otherwise, we get an oscillating graph in the diagram. Please note that for reasons of notation, there is only one single RC circuit which has no deviation, i.e. $\beta = 0$. However, due to the choices made above, it fulfils the mirror symmetry by itself. In this case, the minimum of the imaginary part of the impedance lying on the symmetry axis is reached at $\omega = 1/RC$. Finally, the serial connection of $2N+1$ RC circuits has the parameters:

$$R_n = \frac{R}{2N+1} \tag{29}$$

$$C_n = (2N+1)\,C\tan\left(\frac{\pi}{4} + \frac{n}{N}\cdot\frac{\beta}{2}\right), \tag{30}$$

with the integer $-N \leqslant n \leqslant N$. Moreover, the time constants τ_n of the RC circuits are:

$$\tau_n = R_nC_n = RC\tan\left(\frac{\pi}{4} + \frac{n}{N}\cdot\frac{\beta}{2}\right). \tag{31}$$

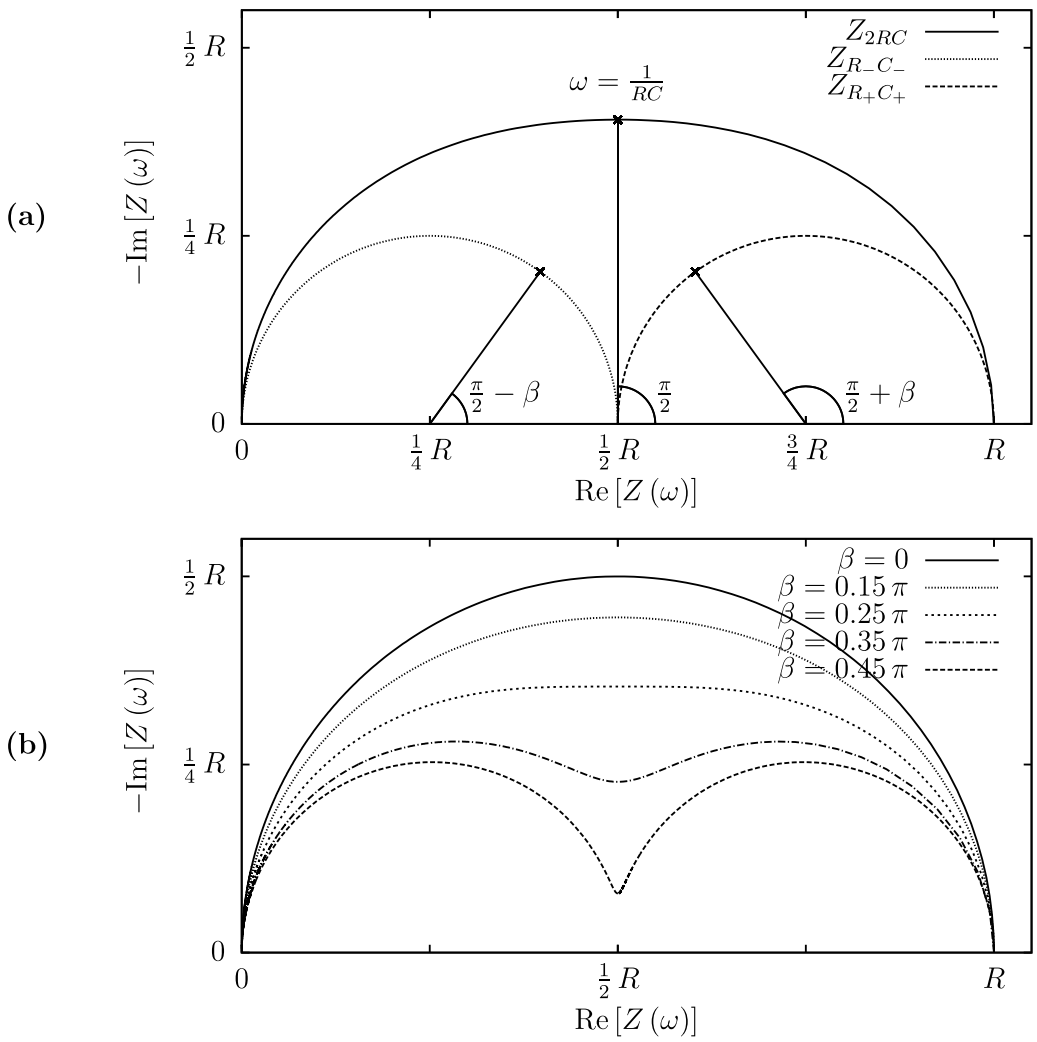

Figure 2. (a) Nyquist plot of the impedance of two RC circuits and their serial connection with identical ohmic resistances $R/2$ and capacitances due to (25) with $\beta = 0.2\,\pi$. The labelled points are all at the frequency $\omega = 1/RC$. (b) Nyquist plots with varying β.

Indeed, the mirror symmetry is maintained due to the theorem in 2.3 and the choice of the capacitances C_n. It is independent of the number of RC circuits. As a consequence, the total impedance of the $2N+1$ RC circuits is:

$$\begin{aligned} Z_N(\omega) &= \sum_{n=-N}^{N} \frac{R_n}{1+\mathrm{i}\,(\omega R_n C_n)} \\ &= \sum_{n=-N}^{N} \frac{R}{2N+1} \cdot \frac{1-\mathrm{i}\,(\omega RC)\tan\left(\frac{\pi}{4}+\frac{n}{N}\cdot\frac{\beta}{2}\right)}{1+(\omega RC)^2\tan^2\left(\frac{\pi}{4}+\frac{n}{N}\cdot\frac{\beta}{2}\right)}. \end{aligned} \tag{32}$$

However, the number of RC circuits influences the depression. The larger the value of N, the more uniform the depression. For that reason, we take the limit $N \to \infty$ and get the impedance $Z_{\mathrm{APP}}(\omega)$ for the impedance of the approximation of the ZARC element,

$$Z_{\mathrm{APP}}(\omega) = \lim_{N\to\infty} Z_N(\omega) = \frac{R}{\beta} \int_{\frac{\pi}{4}-\frac{\beta}{2}}^{\frac{\pi}{4}+\frac{\beta}{2}} \frac{1-\mathrm{i}\,(\omega RC)\tan(x)}{1+(\omega RC)^2\tan^2(x)}\,\mathrm{d}x. \tag{33}$$

Following some analysis and trigonometry using

$$\begin{aligned} &\int \frac{\alpha\cos^2(x) + 2\,\beta\sin(x)\cos(x) + \gamma\sin^2(x)}{a\cos^2(x) + c\sin^2(x)}\,\mathrm{d}x \\ &= \frac{(\alpha-\gamma)\,x - \beta\ln\left(a\cos^2(x) + c\sin^2(x)\right)}{a-c} \\ &\quad + \frac{\gamma a - \alpha c}{\sqrt{ac}\,(a-c)} \arctan\left(\sqrt{\frac{c}{a}}\tan(x)\right), \end{aligned} \tag{34}$$

from Gröbner and Hofreiter [39, p. 124], the real and imaginary parts of $Z_{\mathrm{APP}}(\omega)$ can be computed by:

$$\mathrm{Re}\left[Z_{\mathrm{APP}}(\omega)\right] = \frac{R}{2}\left(1 + \frac{1+(\omega RC)^2}{1-(\omega RC)^2} - \frac{2\ (\omega RC)}{\left(1-(\omega RC)^2\right)\beta} \cdot \arctan\left(\frac{2\ (\omega RC)}{1+(\omega RC)^2}\cdot\tan(\beta)\right)\right), \tag{35}$$

$$\mathrm{Im}\left[Z_{\mathrm{APP}}(\omega)\right] = -\frac{R}{2}\cdot\frac{2\ (\omega RC)}{\left(1-(\omega RC)^2\right)\beta} \cdot \operatorname{artanh}\left(\frac{1-(\omega RC)^2}{1+(\omega RC)^2}\cdot\sin(\beta)\right). \tag{36}$$

For further details of the computation, we refer to appendix E. The maximum of $-\mathrm{Im}\left[Z_{\mathrm{APP}}(\omega)\right]$ is at $\omega RC = 1$ and has the value $R\sin(\beta)/2\ \beta$. A comparison of the two circuits, ZAPP and ZARC, requires an expression connecting α and β. We continue with two possibilities for connection: an equation or a minimization problem. In the following, we let β denote the parameter determined by the equation, while β_{min} stands for the parameter determined by the minimization.

Firstly, we make an ansatz to choose a frequency such that the global imaginary minima of ZAPP and ZARC coincide. Therefore, the two equations:

$$\frac{R}{2}\tan\left(\frac{\alpha}{4}\pi\right) = \frac{R}{2}\frac{\sin(\beta)}{\beta} \tag{37}$$

$$\alpha = \frac{4}{\pi}\arctan\left(\frac{\sin(\beta)}{\beta}\right), \tag{38}$$

are fulfilled. According to the method, $0 \leqslant \beta < \pi/2$ holds true, restricting α to the interval $(4/\pi\cdot\tan(2/\pi) \approx 0.7218, 1\ ]$. Conversely, analytically finding β given α in (38) is not that easy. However, Newton's method is a good tool with which to compute the relation numerically.

Secondly, we minimize the integrated quadratic deviation from ZAPP to ZARC to get the relation between α and β_{min}. This means that we minimize the squared area under the curve $|Z_{\mathrm{APP}}(\omega) - Z_{\mathrm{ARC}}(\omega)|$ using the L^2 norm,

$$\Delta_{\mathrm{APP}} = ||Z_{\mathrm{APP}} - Z_{\mathrm{ARC}}||_2 = \left(\int_0^{+\infty} |Z_{\mathrm{APP}}(\omega) - Z_{\mathrm{ARC}}(\omega)|^2\,\mathrm{d}\omega\right)^{\frac{1}{2}}, \tag{39}$$

and the minimum is:

$$\Delta_{\mathrm{APP,min}} = \min_{0\ \leqslant\beta<\frac{\pi}{2}} ||Z_{\mathrm{APP}} - Z_{\mathrm{ARC}}||_2 = \min_{0\ \leqslant\beta<\frac{\pi}{2}} \left(\int_0^{+\infty} |Z_{\mathrm{APP}}(\omega) - Z_{\mathrm{ARC}}(\omega)|^2\,\mathrm{d}\omega\right)^{\frac{1}{2}}. \tag{40}$$

Figure 3 graphically compares ZARC with the two strategies for determining ZAPP. Figure 3(a) shows the Nyquist diagram of the ZARC element for $\alpha = 0.75$ and its appropriate approximations due to (38) and due to the minimization (40). The figure also shows that the impedance $Z_{\mathrm{APP}}(\omega)$ is uniformly depressed for all β. Moreover, the solid ZAPP and ZARC coincide at the local extrema and have their biggest deviation at the sides. The reason for this is the approximation of ZARC with semicircles. Hence, ZAPP always intersects the real-part axis at an angle of $\pi/2$, whereas the intersection of ZARC is at $\alpha\pi/2$. On the other hand, the dashed ZAPP extremum is below the ZARC extremum, though the deviation is smaller at the sides. Figure 3(b) represents the real and imaginary parts for the case $\alpha = 0.75$. Both the real and imaginary parts almost lie on top of each other. By construction, the areas under the dashed lines, representing the minimization problem in figure 3(c) are smaller than those enclosed by the solid lines. Nevertheless, the deviation between β and β_{min} for the same α is less than $0.01\,\pi$. The relations between α and β and between α and β_{min} are both shown in figure 3(d). Finally, according to figure 3, the minimization method yields slightly better results. However, we prefer the first method, which relates α and β through (38). The equation is a clear expression which can be used for further computation.

Moreover, the limit $N \to \infty$ also offers the opportunity to analytically compute the total ohmic resistance and the total capacitance of the approximal circuits using Kirchhoff's laws,

$$R_{\mathrm{total},N} = \sum_{n=-N}^{N} R_n = \sum_{n=-N}^{N}\frac{R}{2N+1} \to \frac{R}{2}\int_{-1}^{1}\mathrm{d}x = R \tag{41}$$

$$\frac{1}{C_{\mathrm{total},N}} = \sum_{n=-N}^{N}\frac{1}{C_n} = \sum_{n=-N}^{N}\frac{1}{(2N+1)\,C\tan\left(\frac{\pi}{4}+\frac{n}{N}\cdot\frac{\beta}{2}\right)} \to \frac{1}{2\,\beta C}\int_{\frac{\pi}{4}-\frac{\beta}{2}}^{\frac{\pi}{4}+\frac{\beta}{2}}\frac{1}{\tan(x)}\mathrm{d}x = \frac{1}{2\,\beta C}\cdot\ln\left(\frac{1+\sin(\beta)}{1-\sin(\beta)}\right). \tag{42}$$

Regarding condition (a), the result for the total ohmic resistance is clear. Due to the construction of the model, the dependence of the total capacitance on β is evident. According to the equation above, the total capacitance decreases if β increases. C_{total} converges to zero in the limit $\beta \to \pi/2$. Therefore, we can deduce that the more the semi-circle in the Nyquist plot is depressed, the more the total capacitance decreases. In the limit $N \to \infty$, the time constant goes to

$$\tau(x) = RC\tan\left(\frac{\pi}{4}+\frac{\beta}{2}x\right), \tag{43}$$

with $-1 \leqslant x \leqslant 1$. Its range has a total width of $2RC\tan(\beta)$, and the normalized distribution of τ is

$$\rho(\tau) = \frac{1}{2}\frac{\mathrm{d}x}{\mathrm{d}\tau} = \frac{1}{RC\beta}\frac{1}{1+\left(\frac{\tau}{RC}\right)^2}, \tag{44}$$

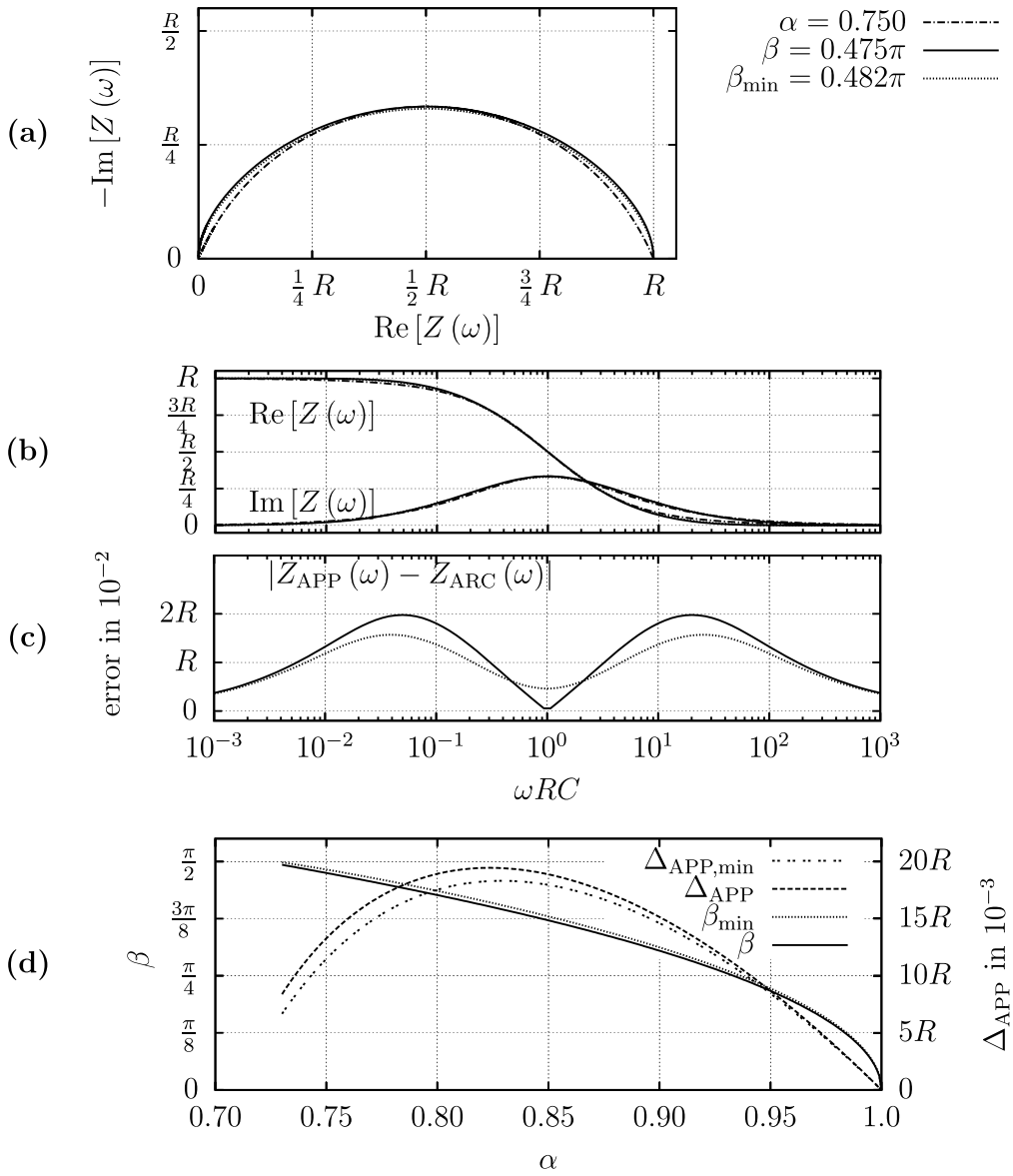

Figure 3. (a) Nyquist plot of ZAPP and ZARC for $\alpha = 0.750$ and $\beta = 0.475\,\pi$, respectively. (b) Real and imaginary parts of ZAPP and ZARC for $\alpha = 0.750$, $\beta = 0.475\,\pi$, and $\beta_{\min} = 0.482\,\pi$ versus the logarithmic scaled frequency. (c) The error $|Z_{\mathrm{APP}}\,(\omega) - Z_{\mathrm{ARC}}\,(\omega)|$ for $\alpha = 0.750$ and their related β and $\beta_{\min}$. (d) β and $\beta_{\min}$ as a function of α due to calculation and optimization and the corresponding deviation Δ_{APP} from ZARC in the L^2 norm.

giving the ratio of RC circuits in the interval $[\tau;\tau + \mathrm{d}\tau]$. Therefore, the number of small time constants decreases for increasing τ. Figure 4 shows the distribution of the time constants and the normalized density for $\beta = 0.35\,\pi$.

Finally, we show that K can be related to the variables R, C, and α. For this, we use the fact that ZARC and ZAPP coincide at the point $(R/2; -R/2 \cdot \tan(\alpha/4\pi))$. From condition (b), it follows that $\omega RC = 1$ holds true at this point. Moreover, ZARC satisfies the condition $\omega^{\alpha} RK = 1$. Plugging these expressions into each other and solving for K leads to a modified capacitance $K = (RC)^{\alpha}/R$, and therefore, the impedance follows:

$$Z_{\mathrm{ARC}}\,(\omega) = \frac{R}{1 + (\mathrm{i}\omega)^{\alpha} RK} = \frac{R}{1 + (\mathrm{i}\omega RC)^{\alpha}}, \tag{45}$$

which is a much more physical expression, since the parameters do not change their units.

2.4.2. Behaviour in the time domain. The origin of the behaviour of ZAPP in the time domain lies in the Laplace transformability of the impedance of a single RC circuit, since (9) connects the voltage response to a current step using the inverse Laplace transform of the impedance. From that, we can deduce the properties of ZAPP in the time domain. It is well known that

$$U_{RC}\,(t) = RI\left(1 - \mathrm{e}^{-\frac{t}{RC}}\right), \tag{46}$$

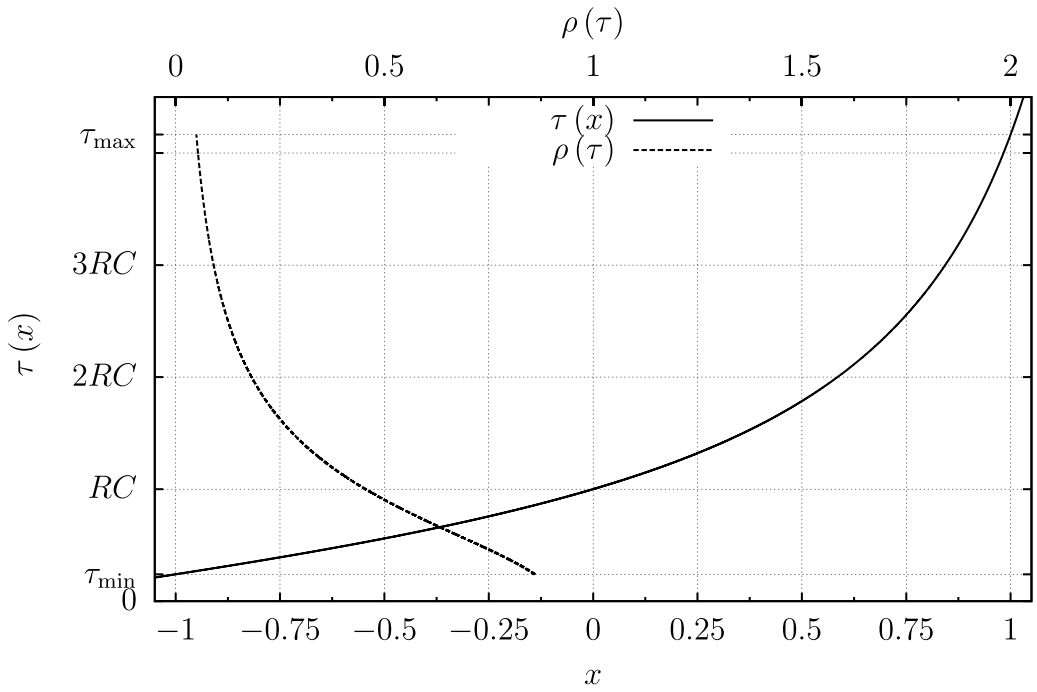

Figure 4. The solid line represents the distribution of the time constants for $\beta = 0.35\,\pi$ and uses the lower x-axis. The upper x-axis belongs to the normalized density, which is dashed.

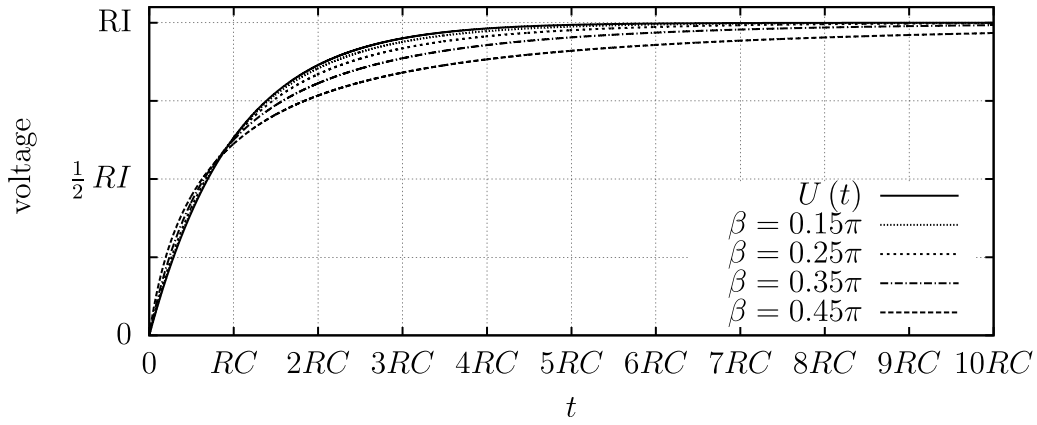

Figure 5. Voltage responses to a current step of ZAPP for different β and the response of a single RC circuit.

is the reaction of an RC circuit to a current step at $t = 0$ with an amplitude $I \neq 0$. Without loss of generality, we set $I > 0$. The approximation of the ZARC element that uses a number of RC circuits converging to infinity behaves as follows:

$$U_{\mathrm{APP}}(t) = \lim_{N\to\infty} \sum_{n=-N}^{N} R_n I \left(1 - \mathrm{e}^{-\frac{t}{R_n C_n}}\right) = \frac{It}{\beta C} \int_{\frac{t}{RC}\tan\left(\frac{\pi}{4}-\frac{\beta}{2}\right)}^{\frac{t}{RC}\tan\left(\frac{\pi}{4}+\frac{\beta}{2}\right)} \frac{1-\mathrm{e}^{-u}}{\left(\frac{t}{RC}\right)^2 + u^2}\,\mathrm{d}u. \tag{47}$$

However, it cannot be computed analytically, so we need to approximate the integral using the sum. As a consequence of the parameter choices, the behaviour of the curve $U_{\mathrm{APP}}(t)$ compared to $U_{RC}(t)$ is intuitive. For increasing β, the interval of all time constants $[RC\tan(\pi/4 - \beta/2); RC\tan(\pi/4 + \beta/2)]$ becomes wider. The contribution of time constants smaller than $\tau = RC$ results in a faster growth of $U_{\mathrm{APP}}(t)$ for small times, whereas time constants larger than τ flatten the graph faster for $t > RC$, compared to $U_{RC}(t)$. In figure 5, we show the voltage responses for different β. The product of the ohmic resistance R and the current I gives the total voltage delta. The capacitance C influences the gradient of the function at the beginning and β influences its curvature.

2.5. Approximation of a ZARC element with three RC circuits

2.5.1. Approximation in the frequency domain. In contrast to the method above and Brug's [6] ansatz, we now use three RC

circuits with different ohmic resistances and different capacitances. Two of the RC circuits have equal ohmic resistances $R_{2\pm}$ which are, in general, different from the ohmic resistance R_1 of the remaining circuit. The additional degree of freedom has to be compensated for by a minimization problem. Nevertheless, $R = R_1 + R_{2+} + R_{2-}$ is fulfilled. Moreover, we also set the approximation equal to the ZARC element at the maximum of $-\mathrm{Im}\left[Z_{\mathrm{ARC}}(\omega)\right]$. For symmetry reasons, the frequency of this point satisfies $\omega^{\alpha} RK = 1 = \omega RC = \omega R_1 C_1$, where C is a reference capacitance, which is used later on to relate all three capacitances and to determine the total capacitance of the equivalent electrical circuit. According to this assumption and (25), the single capacitances are:

$$C_1 = \frac{R}{R_1}\, C \tag{48}$$

$$C_{2\pm} = \frac{R}{R_{2\pm}}\, C \tan\left(\frac{\pi}{4} \pm \frac{\xi}{2}\right). \tag{49}$$

Here, ξ is the parameter that regulates all other quantities of the approximation and correlates with α. From the symmetry, we know that at the minimum of the imaginary part,

$$\frac{R_1}{2} + \frac{R_{2+}}{2} \sin\left(\frac{\pi}{2} + \xi\right) + \frac{R_{2-}}{2} \sin\left(\frac{\pi}{2} - \xi\right) = \frac{R}{2} \tan\left(\frac{\alpha}{4}\pi\right), \tag{50}$$

is satisfied and, therefore,

$$R_1 = R\, \frac{\tan\left(\frac{\alpha}{4}\pi\right) - \sin\left(\frac{\pi}{2} - \xi\right)}{1 - \sin\left(\frac{\pi}{2} - \xi\right)} \tag{51}$$

$$R_{2\,\pm} = \frac{R}{2}\, \frac{1 - \tan\left(\frac{\alpha}{4}\pi\right)}{1 - \sin\left(\frac{\pi}{2} - \xi\right)}. \tag{52}$$

Finally, we get the total impedance for the serial connection of the three RC circuits:

$$\begin{aligned} Z_{3RC}(\omega) &= \frac{R_1}{1 + \mathrm{i}\,(\omega R_1 C_1)} + \frac{R_{2+}}{1 + \mathrm{i}\,(\omega R_{2+} C_{2+})} + \frac{R_{2-}}{1 + \mathrm{i}\,(\omega R_{2-} C_{2-})} \\ &= \frac{R\, \frac{\tan\left(\frac{\alpha}{4}\pi\right) - \sin\left(\frac{\pi}{2} - \xi\right)}{1 - \sin\left(\frac{\pi}{2} - \xi\right)}}{1 + \mathrm{i}\,(\omega RC)} + \frac{\frac{R}{2}\, \frac{1 - \tan\left(\frac{\alpha}{4}\pi\right)}{1 - \sin\left(\frac{\pi}{2} - \xi\right)}}{1 + \mathrm{i}\left(\omega RC \tan\left(\frac{\pi}{4} + \frac{\xi}{2}\right)\right)} \\ &\quad + \frac{\frac{R}{2}\, \frac{1 - \tan\left(\frac{\alpha}{4}\pi\right)}{1 - \sin\left(\frac{\pi}{2} - \xi\right)}}{1 + \mathrm{i}\left(\omega RC \tan\left(\frac{\pi}{4} - \frac{\xi}{2}\right)\right)}. \end{aligned} \tag{53}$$

Analogously to the minimization method above in (39), we determine the dependence of ξ on α by:

$$\begin{aligned} \Delta_{3RC,\min} &= \min_{0 \leqslant \xi < \frac{\pi}{2}} ||Z_{3RC} - Z_{\mathrm{ARC}}||_2 \\ &= \min_{0 \leqslant \xi < \frac{\pi}{2}} \left(\int_0^{\infty} |Z_{3RC}(\omega) - Z_{\mathrm{ARC}}(\omega)|^2 \,\mathrm{d}\omega \right)^{\frac{1}{2}}. \end{aligned} \tag{54}$$

Moreover, due to Kirchhoff's law, we can compute the total ohmic resistance and the total capacitance. By definition, the total ohmic resistance is R. The total capacitance is

$$\begin{aligned} \frac{1}{C_{\mathrm{tot,3RC}}} &= \frac{1}{C_1} + \frac{1}{C_{2+}} + \frac{1}{C_{2-}} \\ &= \left(1 + \frac{1 - \tan\left(\frac{\alpha}{4}\pi\right)}{\sin\left(\frac{\pi}{2} - \xi\right)}\right) \frac{1}{C}, \end{aligned} \tag{55}$$

which equals C for $\alpha = 1$ since, in this case, ZARC is identical to an RC circuit.

2.5.2. Behaviour in the time domain. The computation of the behaviour of $Z_{3RC}(\omega)$ in the time domain can be deduced from the behaviour of each RC circuit (46). The three time constants are:

$$\tau_1 \quad = R_1 C_1 = RC \tag{56}$$

$$\tau_{2\,\pm} = R_{2\,\pm} C_{2\,\pm} = RC \tan\left(\frac{\pi}{4} \pm \frac{\xi}{2}\right), \tag{57}$$

where $\tau_{2-} < \tau_1 < \tau_{2+}$, and therefore, the voltage response to a current step of amplitude I is:

$$\begin{aligned} U_{3RC}(t) &= R_1 I \left(1 - \mathrm{e}^{-\frac{t}{\tau_1}}\right) + R_{2+} I \left(1 - \mathrm{e}^{-\frac{t}{\tau_{2+}}}\right) \\ &\quad + R_{2-} I \left(1 - \mathrm{e}^{-\frac{t}{\tau_{2-}}}\right) \\ &= \frac{RI}{2\left(1 - \sin\left(\frac{\pi}{2} - \xi\right)\right)} \left(\left(\tan\left(\frac{\alpha}{4}\pi\right) - \sin\left(\frac{\pi}{2} - \xi\right)\right) \right. \\ &\quad \times \left(1 - \mathrm{e}^{-\frac{t}{RC}}\right) + \left(1 - \tan\left(\frac{\alpha}{4}\pi\right)\right) \left(1 - \mathrm{e}^{-\frac{t}{RC\tan\left(\frac{\pi}{4} + \frac{\xi}{2}\right)}}\right) \\ &\quad \left. + \left(1 - \tan\left(\frac{\alpha}{4}\pi\right)\right) \left(1 - \mathrm{e}^{-\frac{t}{RC\tan\left(\frac{\pi}{4} - \frac{\xi}{2}\right)}}\right) \right). \end{aligned} \tag{58}$$

The $R_{2-}C_{2-}$ circuit reacts first to the current step, then follows $R_1 C_1$ with the biggest voltage delta and finally the $R_{2+}C_{2+}$ circuit contributes for large times.

2.6. Comparison of the two approaches with ZARC

In this part, we graphically compare the two approaches from 2.4 and 2.5 with the ZARC element. We start with the comparison of ZAPP and Z_{3RC} in the frequency domain. Therefore, we choose $\alpha = 0.750$, such that ZARC deviates greatly from a pure RC circuit. Figure 6(a) shows the Nyquist diagram of ZARC and ZAPP with $\beta = 0.475\,\pi$ according to (38) and Z_{3RC} with $\xi = 0.397\,\pi$, as determined by minimization. Due to (48)–(52), the parameters have the following values:

$R_1 = 0.514\,R$, $R_{2\,\pm} = 0.243\,R$, $C_1 = 1.95\,C$, $C_{2+} = 15.3\,C$ and $C_{2-} = 0.408\,C$.

By construction, all graphs meet at the origin of the coordinates, at the point $(R;0)$ and at the maximum of $-\mathrm{Im}\left[Z_{\mathrm{ARC}}(\omega)\right]$. Furthermore, ZAPP, with a uniform

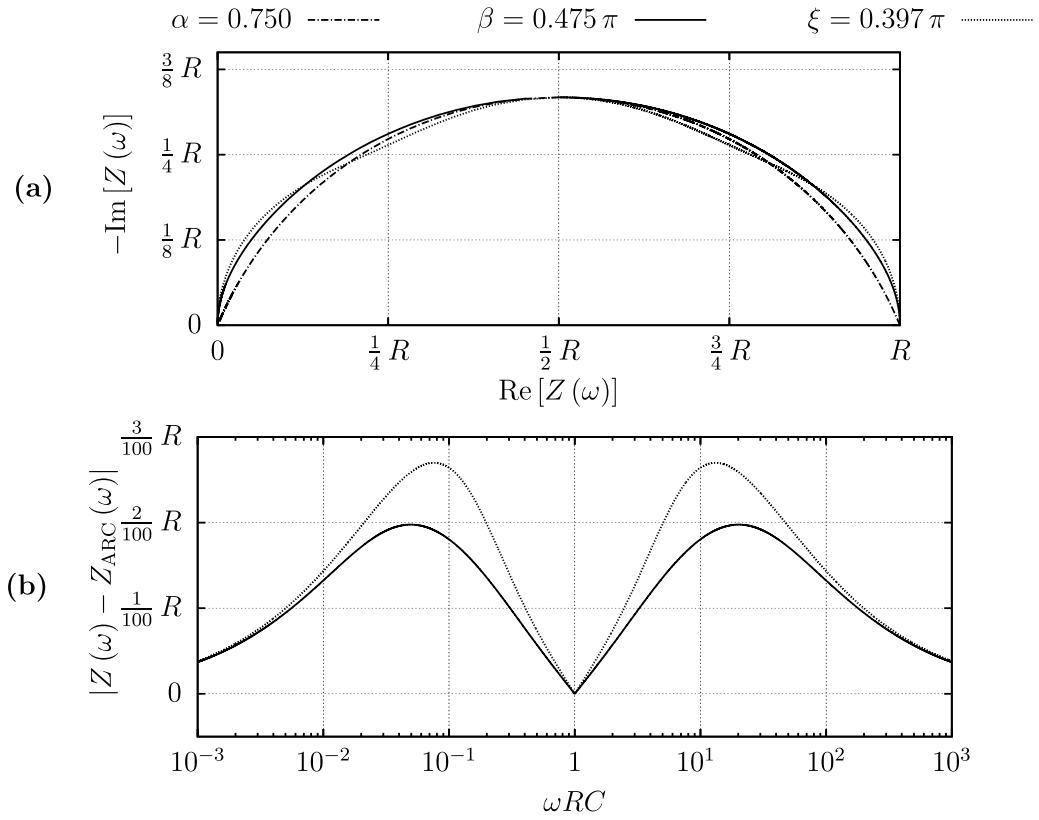

Figure 6. (a) Nyquist diagram of ZARC with $\alpha = 0.750$, of ZAPP with $\beta = 0.475\,\pi$ and of Z_{3RC} with $\xi = 0.397\,\pi$. (b) Absolute deviation of ZAPP and Z_{3RC} from ZARC with the corresponding parameters.

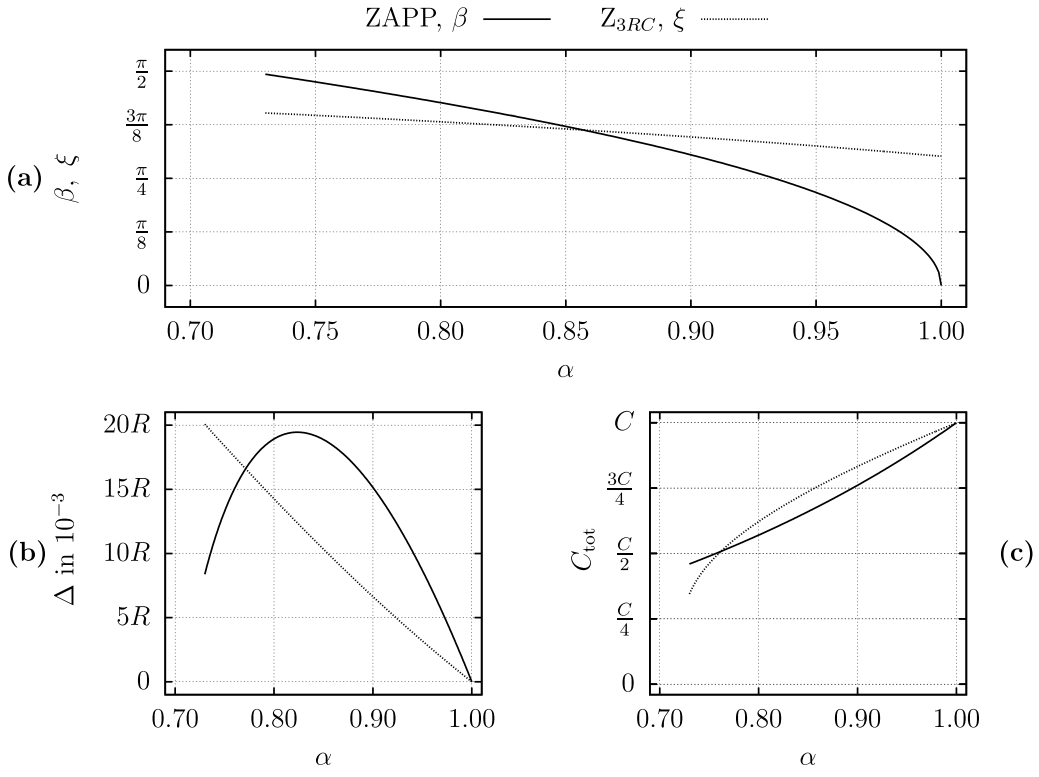

Figure 7. (a) Relation between the parameter α of ZARC and β of ZAPP; also, between α and ξ of Z_{3RC}. (b) L^2 norm of $Z_{\mathrm{APP}} - Z_{\mathrm{ARC}}$ and $Z_{\mathrm{APP}} - Z_{3RC}$. (c) Total capacitance of the equivalent circuits ZAPP and Z_{3RC}.

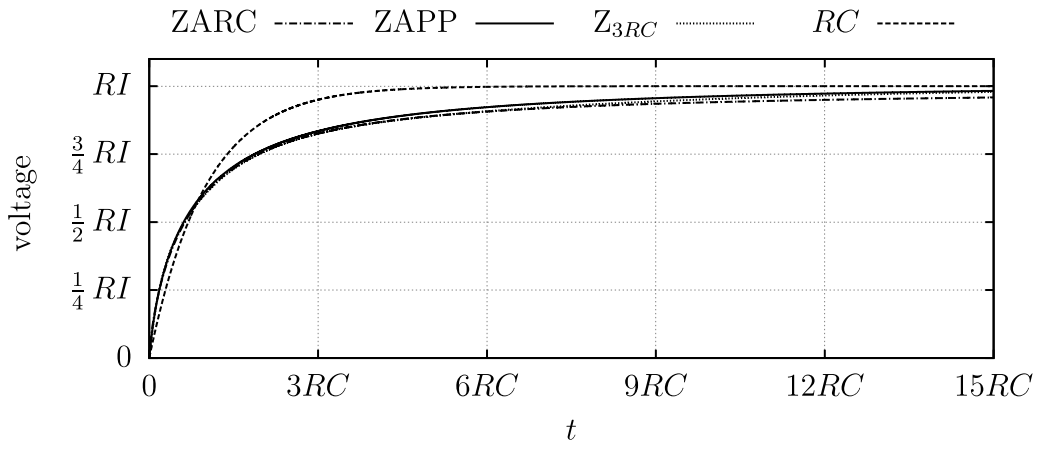

Figure 8. Voltage response to a current step with an amplitude I of ZAPP with $\beta = 0.475\,\pi$, Z_{3RC} with $\xi = 0.397\,\pi$ and a simple RC circuit as approximations for ZARC with $\alpha = 0.750$.

curvature, is always above ZARC, while Z_{3RC} intersects the graph of ZARC twice. Figure 6(b) shows the logarithmically scaled deviations $|Z_{\mathrm{APP}}(\omega) - Z_{\mathrm{ARC}}(\omega)|$ and $|Z_{3RC}(\omega) - Z_{\mathrm{ARC}}(\omega)|$. The graphs are symmetric up to the frequency $\omega RC = 1$, based on relation (28), between the frequencies of the angles φ and $\pi - \varphi$. They are zero at $\omega RC = 1$ and show a similar behaviour. The maximal deviation of the two graphs is less than $0.01\,R$.

Figure 7 (a), shows the relation between α and β, and α and ξ. The parameter β goes to zero when α goes to one. As a consequence, all infinitely many RC circuits are identical. In the case of the approximation with three RC circuits, both the $R_2\,{\pm}C_2\,{\pm}$-circuits vanish and ξ is arbitrary. Moreover, in figure 7 (b), we show the absolute deviation of ZARC from ZAPP and that of ZARC from Z_{3RC}. The approximation of the ZARC element with three RC circuits has smaller deviations from ZARC than from ZAPP in the interval $[0.77; 1\,]$, which is due to the varying ohmic resistances. Furthermore, figure 7 (c) presents the total capacitance of the two equivalent electrical circuits with respect to α. Both graphs show that for $\alpha < 1$, the total capacitance is also reduced. Therefore, the parameter α influences not only the single capacitances, but also the total capacitance of the equivalent circuit.

Finally, figure 8 shows the almost identical response of ZAPP, Z_{3RC}, and ZARC in the time domain to a current step for $\alpha = 0.750$, $\beta = 0.475\,\pi$, and $\xi = 0.397\,\pi$. A comparison is made with a single RC circuit, which satisfies $\alpha = 1$.

3. Validation of the models

In order to validate the two approaches, we fit ZAPP and Z_{3RC} to the impedance measurement data and compare the results to the parameters from the fit of the ZARC element. Here, we present impedance measurement data from three high-energy lithium-ion cells, Molicel IHR18650A by E-One Moli Energy Corp., with a nominal capacity of 1.95 Ah. The anode material is graphite, and lithium–cobalt–nickel–manganese oxide is the cathode material. The impedance was measured after charging the cells to a 50 % state of charge and relaxing them for three hours. Schuster *et al* describe the measurements in detail in [40].

In general, the measurement data describe a superposition of all processes which occur in the cell. They can be summed up as the contributions of inductive effects, ohmic resistances, the solid electrolyte interphase, the charge transfer, and the diffusion processes [41]. Here, we model the charge transfer, which is interpreted as the data starting on the right side of the semicircle, see 10. Moreover, all three cells have $\alpha \approx 0.72$, such that the deviation from an RC circuit is maximal for ZAPP.

We use a nonlinear least-squares Marquardt–Levenberg algorithm to fit the imaginary parts of the different models to the corresponding measurement data and to determine the corresponding parameters. Furthermore, the parameters are used to compute the real parts and to show that the measurement data satisfy the Kramers–Kronig relation. Finally, the Nyquist diagrams of the different models can be compared to the measurement data. The results are shown in figures 9 and 10.

Moreover, we present a table of the parameters of cell C and the parameters R, C and α derived from them. Both the figures and the table show that the parameters of the fit of ZAPP and ZARC are almost identical in the considered frequency range between 10 Hz and 300 Hz. According to figure 7 (b), Z_{3RC} deviates more from ZARC than from ZAPP for $\alpha \approx 0,72$; see figure 10. Table 1 presents the parameters from the fit of cell C's measurement data. Additionally, we present a comparison of the relevant parameters obtained from $K = (RC)^{\alpha}/R$, (38) and figure 7 (a). The parameters of ZAPP and ZARC coincide, whereas the parameters of Z_{3RC} deviate.

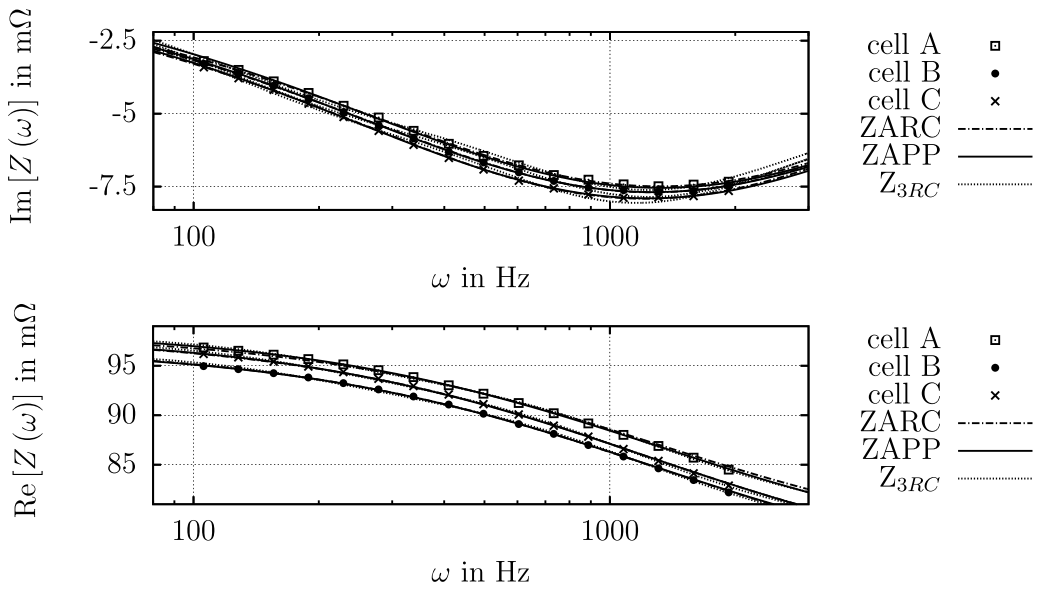

Figure 9. Real and imaginary parts of the measurement data from cells A, B and C and the appropriate approximations ZARC, ZAPP, and Z_{3RC}. The imaginary parts of the models were fitted to the imaginary part of the measurement data and the behaviour of the real parts follows from this.

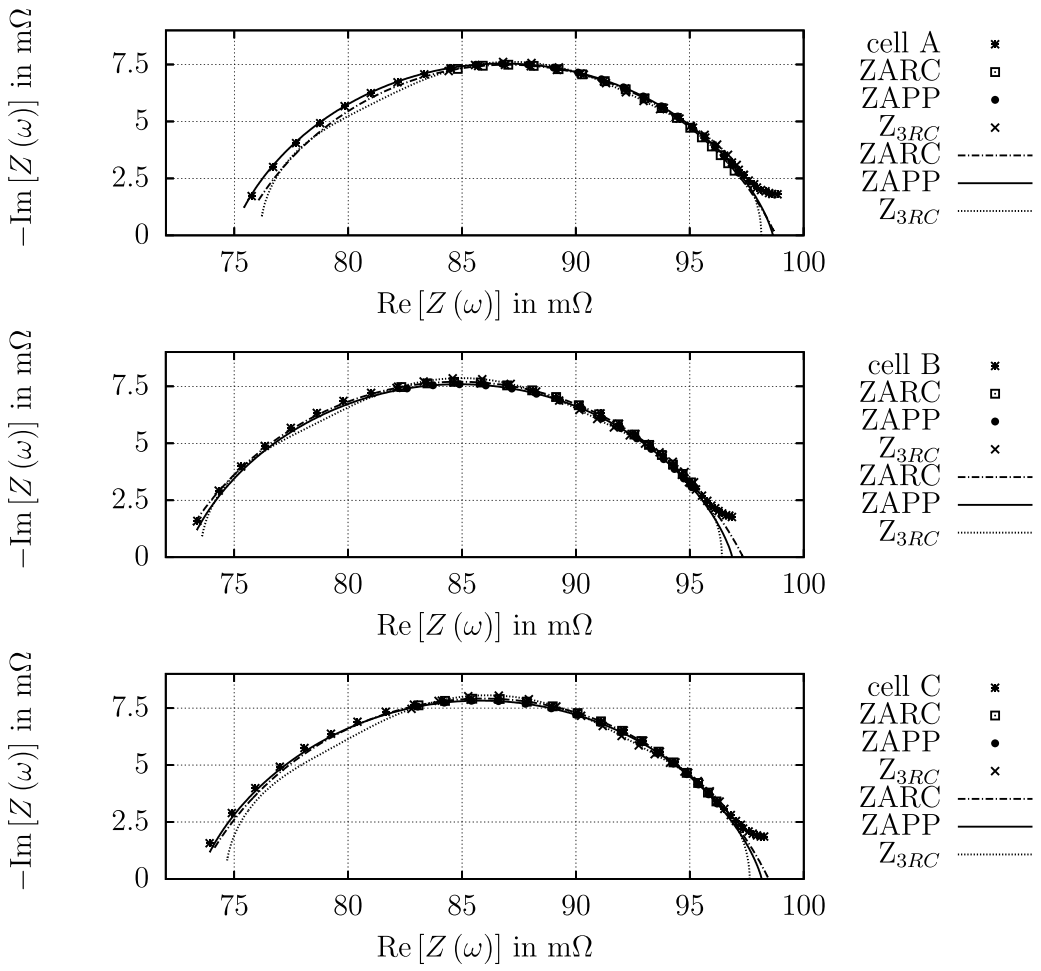

Figure 10. Nyquist diagram of the measurement data of three cells A, B, and C and the corresponding models ZAPP, ZARC, and Z_{3RC}.

Table 1. Parameters derived from the fit of cell C's measurement data to ZARC, ZAPP, and Z_{3RC}. The second line contains the corresponding values for R, C, and α.

	ZARC	ZAPP	Z_{3RC}
	$R = 0.0250\,\Omega$	$R = 0.0247\,\Omega$	$R = 0.0230\,\Omega$
	$K = 0.251\,^{\mathrm{As}^{\alpha}}/\mathrm{V}$	$C = 0.0330\,^{\mathrm{As}}/\mathrm{V}$	$C = 0.0376\,^{\mathrm{As}}/\mathrm{V}$
	$\alpha = 0.714$	$\beta = 0.499\,\pi$	$\xi = 0.397\,\pi$
vs.	$R = 0.0250\,\Omega$	$R = 0.0247\,\Omega$	$R = 0.0230\,\Omega$
	$C = 0.0329\,^{\mathrm{As}}/\mathrm{V}$	$C = 0.0330\,^{\mathrm{As}}/\mathrm{V}$	$C = 0.0376\,^{\mathrm{As}}/\mathrm{V}$
	$\alpha = 0.714$	$\alpha = 0.722$	$\alpha = 0.748$

4. Conclusions

The ZARC element is a mathematical object that describes measured data very well. In this paper, we translated this mathematical object into the language of electrical engineering without any optimization algorithm. In doing so, we approximated the ZARC element using RC circuits that modelled a dynamic system with unique time constants. Finally, we compared the results in the frequency and time domains.

In this paper, we proved a theorem verifying the mirror-symmetric impedance of two serially connected RC circuits in a Nyquist diagram, given the condition that both ohmic resistances are equal to each other. On the one hand, we showed that the ansatz of Brug *et al* in [6], which is to use identical ohmic resistances but varying capacitances, is possible and can be done by hand. Therefore, we introduced a new ZAPP model to approximate a ZARC element with infinitely many RC circuits. The origin of the model depends on some analysis, but does not require an optimisation algorithm. Moreover, this model can be used to approximate the ZARC element for all continuous values of $\alpha \in (0.722, 1]$. In total, we only need the three parameters R, C, and β to determine the model. Here, R is an ohmic resistance, and C is the capacitance of a capacitor. The variable β is connected to the well-known α by an explicit equation. Generally, it is a measure of the distribution of the single capacitances and hence a measure of the deviation of ZAPP from the behaviour of a single RC circuit. Furthermore, β is restricted to the interval $[0, \pi/2)$.

On the other hand, we used the approach of approximating ZARC with three RC circuits, where all parameters varied. However, this degree of freedom required a minimization problem to relate α to the equivalent of β, called ξ, on which all parameters depended.

Moreover, we used an example to show that the new approaches can be used to model the charge transfer of lithium-ion cells and replace ZARC. Here, the results of ZAPP are more precise than those of Z_{3RC}.

Additionally, we realised that both approximations have decreasing total capacitances for decreasing α.

Finally, we presented the influences of α, β, and ξ of ZARC, ZAPP, and Z_{3RC}, respectively, in the time domain. For decreasing α and appropriate values of β and ξ, the curvature of the voltage response to a current step is stronger than that of a single RC circuit.

Despite this, this approach can also be used to approximate a ZARC element with five serially connected RC circuits. The results will be better, especially for smaller α. However, additional conditions are required, which significantly increase the computational effort. Furthermore, the method can be transferred to all types of equivalent electrical circuits that deviate from a semicircle in the Nyquist diagram, e.g., RL circuits.

Data availability statement

The data generated and/or analysed during the current study are not publicly available for legal/ethical reasons but are available from the corresponding author on reasonable request.

Acknowledgments

The work presented here was financially supported by the German Federal Ministry for Economic Affairs and Energy (BMWi) under Grant No. 03ETE019F (LImeS). The authors further thank Elisabeth Gillich for her excellent support reviewing this manuscript.

Appendix A. Computation in detail: the ZARC element

In the appendix, we show the computation mentioned above in detail.

We start with the ZARC element satisfying the equation for a circle. Let $x = \frac{\alpha}{2}\pi$ and $y = \omega^{\alpha} RK$; then

$$
\begin{aligned}
&\left(\mathrm{Re}\left[Z_{\mathrm{ZARC}}(\omega)\right]-\frac{R}{2}\right)^2+\left(\mathrm{Im}\left[Z_{\mathrm{ZARC}}(\omega)\right]-\frac{R}{2}\cdot\frac{\cos(x)}{\sin(x)}\right)^2\\
&=\left(\frac{1+y\cos(x)}{1+2y\cos(x)+y^2}R-\frac{R}{2}\right)^2+\left(\frac{-y\sin(x)}{1+2y\cos(x)+y^2}R-\frac{R}{2}\cdot\frac{\cos(x)}{\sin(x)}\right)^2\\
&=\frac{R^2}{4}\cdot\left(\frac{2+2y\cos(x)-1-2y\cos(x)-y^2}{1+2y\cos(x)+y^2}\right)^2+\frac{R^2}{4}\cdot\left(\frac{2y\sin^2(x)+\cos(x)+2y\cos^2(x)+y^2\cos(x)}{(1+2y\cos(x)+y^2)\sin(x)}\right)^2\\
&=\frac{R^2\left(\sin^2(x)\left(1-y^2\right)^2+4y^2+4y\cos(x)\left(1+y^2\right)+\cos^2(x)\left(1+y^2\right)^2\right)}{4\sin^2(x)\left(1+2y\cos(x)+y^2\right)^2}\\
&=\frac{R^2\left(1+y^4+2y^2\left(\cos^2(x)-\sin^2(x)+2\right)+4y\cos(x)\left(1+y^2\right)\right)}{4\sin^2(x)\left(1+2y\cos(x)+y^2\right)^2}\\
&=\frac{R^2\left(1+2y^2+y^4+(2y\cos(x))^2+4y\cos(x)\left(1+y^2\right)\right)}{4\sin^2(x)\left(1+2y\cos(x)+y^2\right)^2}=\frac{R^2\left(\left(1+y^2\right)^2+(2y\cos(x))^2+4y\cos(x)\left(1+y^2\right)\right)}{4\sin^2(x)\left(1+2y\cos(x)+y^2\right)^2}\\
&=\frac{R^2(x)\left(1+2y\cos(x)+y^2\right)^2}{4\sin^2(x)\left(1+2y\cos(x)+y^2\right)^2}=\left(\frac{R}{2\sin(x)}\right)^2.
\end{aligned}
\tag{A.1}
$$

Appendix B. Computation in detail: time behaviour of ZARC element

In order to compute the voltage response to a current step in 2.2, equation (9), we rearrange Heaviside's definition of impedance,

$$
Z(z)=\frac{\mathcal{L}\{U(t)\}(z)}{\mathcal{L}\{\mathrm{I}(t)\}(\mathrm{z})},
\tag{B.1}
$$

to

$$
\begin{aligned}
U(t)&=\mathcal{L}^{-1}\{Z(z)\cdot\mathcal{L}\{I(\tilde{t})\}(\mathrm{z})\}(t)\\
&=\mathcal{L}^{-1}\left\{\mathcal{L}\left\{\left(\mathcal{L}^{-1}\{Z(\tilde{z})\}*I\right)(\tilde{t})\right\}(z)\right\}(t)\\
&=\left(\mathcal{L}^{-1}\{Z(z)\}*I\right)(t)\\
&=\int_0^t\mathcal{L}^{-1}\{Z(z)\}(\tilde{t})\cdot I\cdot\Theta(t-\tilde{t})\,\mathrm{d}\tilde{t}\\
&=I\int_0^t\mathcal{L}^{-1}\{Z(z)\}(\tilde{t})\,\mathrm{d}\tilde{t},
\end{aligned}
\tag{B.2}
$$

where $*$ expresses the convolution and Θ is the Heaviside step function. Consequently, we need to determine the inverse Laplace transform of the ZARC element (10) to compute the voltage response. In this case, we make the educated guess,

$$
\mathcal{L}^{-1}\{Z_{\mathrm{ZARC}}(z)\}(t)=\frac{1}{K}t^{\alpha-1}\sum_{n=0}^{\infty}\frac{1}{\Gamma((n+1)\alpha)}\left(-\frac{t^\alpha}{RK}\right)^n,
\tag{B.3}
$$

since,

$$
\begin{aligned}
&\mathcal{L}\left\{\mathcal{L}^{-1}\{Z_{\mathrm{ZARC}}(z)\}(t)\right\}(\mathrm{z})\\
&=\int_0^\infty\mathrm{e}^{-zt}at^{\alpha-1}\sum_{n=0}^{\infty}\frac{1}{\Gamma((n+1)\alpha)}\left(-\frac{t^\alpha}{b}\right)^n\mathrm{d}t\\
&=a\sum_{n=0}^{\infty}\frac{1}{(-b)^n\Gamma((n+1)\alpha)}\int_0^\infty\mathrm{e}^{-zt}t^{(n+1)\alpha-1}\mathrm{d}t\\
&=a\sum_{n=0}^{\infty}\frac{1}{(-b)^n\Gamma((n+1)\alpha)}\int_0^\infty\mathrm{e}^{-zt}\frac{(zt)^{(n+1)\alpha-1}}{z^{(n+1)\alpha-1}}\frac{\mathrm{d}(zt)}{z}\\
&=a\sum_{n=0}^{\infty}\frac{1}{(-b)^n\Gamma((n+1)\alpha)}\frac{\Gamma((n+1)\alpha)}{z^{(n+1)\alpha}}\\
&=a(-b)\sum_{n=0}^{\infty}\frac{1}{(-bz^\alpha)(-bz^\alpha)^n}\\
&=\frac{a(-b)}{-bz^\alpha}\sum_{n=0}^{\infty}\frac{1}{(-bz^\alpha)^n}\\
&=\frac{ab}{bz^\alpha}\frac{1}{1-\frac{1}{-bz^\alpha}}=\frac{ab}{1+bz^\alpha},
\end{aligned}
\tag{B.4}
$$

with $a=1/K$ and $b=RK$, where we also used:

$$
\Gamma(x)=\int_0^\infty\mathrm{e}^{-t}t^{x-1}\mathrm{d}t
\tag{B.5}
$$

$$\sum_{n=0}^{\infty} x^n = \frac{1}{1-x}. \tag{B.6}$$

Therefore, using $\Gamma(x+1) = x\Gamma(x)$, the voltage response of the ZARC element to a current step, (see (11)), is:

$$\begin{aligned} U_{\mathrm{ARC}}(t) &= I \int_0^t \mathcal{L}^{-1}\{Z_{\mathrm{ARC}}(z)\}(\tilde{t})\,\mathrm{d}\tilde{t} \\ &= I \int_0^t \frac{1}{K}\tilde{t}^{\alpha-1} \sum_{n=0}^{\infty} \frac{1}{\Gamma((n+1)\alpha)} \left(-\frac{\tilde{t}^{\alpha}}{RK}\right)^n \mathrm{d}\tilde{t} \\ &= RI \sum_{n=0}^{\infty} \frac{(-1)^n}{(RK)^{n+1}\Gamma((n+1)\alpha)} \int_0^t \tilde{t}^{(n+1)\alpha-1}\mathrm{d}\tilde{t} \\ &= RI \sum_{n=0}^{\infty} \frac{(-1)^n}{(RK)^{n+1}\Gamma((n+1)\alpha)} \cdot \frac{t^{(n+1)\alpha}}{(n+1)\alpha} \\ &= RI \sum_{n=0}^{\infty} \frac{(-1)^n t^{(n+1)\alpha}}{(RK)^{n+1}\Gamma((n+1)\alpha+1)}. \end{aligned} \tag{B.7}$$

Appendix C. Computation in detail: one RC circuit

In order to compute (14), we take

$$\begin{aligned} \tan(\varphi) &= \frac{-\mathrm{Im}[Z(\omega)]}{\mathrm{Re}[Z(\omega)] - \frac{R}{2}} = \frac{\frac{\omega R^2 C}{1+(\omega RC)^2}}{\frac{R}{1+(\omega RC)^2} - \frac{R}{2}} \\ &= \frac{2\,\omega RC}{1-(\omega RC)^2}, \end{aligned} \tag{C.1}$$

and use

$$\tan(2\,\nu) = \frac{2\,\tan(\nu)}{1-\tan^2(\nu)}. \tag{C.2}$$

Equation (15) follows from

$$\begin{aligned} Z_{RC}(\varphi) &= \frac{R}{1+\mathrm{i}\omega(\varphi)RC} = \frac{R}{1+\mathrm{i}\tan\left(\frac{\varphi}{2}\right)} \\ &= R\left(\cos^2\left(\frac{\varphi}{2}\right) - \mathrm{i}\sin\left(\frac{\varphi}{2}\right)\cos\left(\frac{\varphi}{2}\right)\right) \\ &= \frac{R}{2}\left(1+\cos(\varphi) - \mathrm{i}\sin(\varphi)\right) = \frac{R}{2}\left(1+\mathrm{e}^{-\mathrm{i}\varphi}\right), \end{aligned} \tag{C.3}$$

with

$$\cos^2(\nu) = \frac{1+\cos(2\,\nu)}{2} \tag{C.4}$$

$$\cos(\nu)\sin(\nu) = \frac{\sin(2\,\nu)}{2}. \tag{C.5}$$

Appendix D. Computation in detail: two RC circuits

The computation of the impedance of two serially connected RC circuits which depend on φ_+ and φ_- from (17) is as follows:

$$\begin{aligned} Z_{2RC}(\varphi_+,\varphi_-) &= \frac{R}{4}\left(1+\mathrm{e}^{-\mathrm{i}\varphi_+}\right) + \frac{R}{4}\left(1+\mathrm{e}^{-\mathrm{i}\varphi_-}\right) \\ &= \frac{R}{4}\left(2+\mathrm{e}^{-\mathrm{i}\varphi_+}+\mathrm{e}^{-\mathrm{i}\varphi_-}\right) \\ &= \frac{R}{4}\left(2+\left(\mathrm{e}^{-\mathrm{i}\frac{\varphi_+-\varphi_-}{2}} + \mathrm{e}^{i\frac{\varphi_+-\varphi_-}{2}}\right)\cdot \mathrm{e}^{-\mathrm{i}\frac{\varphi_++\varphi_-}{2}}\right) \\ &= \frac{R}{2}\left(1+\cos\left(\frac{\varphi_+-\varphi_-}{2}\right)\cdot \mathrm{e}^{-\mathrm{i}\frac{\varphi_++\varphi_-}{2}}\right). \end{aligned} \tag{D.1}$$

Furthermore, the total angle φ at vertex $(R/2;0)$ is:

$$\begin{aligned} \tan(\varphi) &= \frac{-\mathrm{Im}[Z_{2RC}(\varphi_+,\varphi_-)]}{\mathrm{Re}[Z_{2RC}(\varphi_+,\varphi_-)] - \frac{R}{2}} \\ &= \frac{\frac{R}{2}\cos\left(\frac{\varphi_+-\varphi_-}{2}\right)\sin\left(\frac{\varphi_++\varphi_-}{2}\right)}{\frac{R}{2}\left(1+\cos\left(\frac{\varphi_+-\varphi_-}{2}\right)\cos\left(\frac{\varphi_++\varphi_-}{2}\right)\right) - \frac{R}{2}} \\ &= \tan\left(\frac{\varphi_++\varphi_-}{2}\right) = \frac{\tan\left(\frac{\varphi_+}{2}\right)+\tan\left(\frac{\varphi_-}{2}\right)}{1-\tan\left(\frac{\varphi_+}{2}\right)\tan\left(\frac{\varphi_-}{2}\right)} \\ &= \frac{(\omega R_+C_+)+(\omega R_-C_-)}{1-(\omega R_+C_+)(\omega R_-C_-)}, \end{aligned} \tag{D.2}$$

using the trigonometric relation:

$$\tan(\nu+\mu) = \frac{\tan(\nu)+\tan(\mu)}{1-\tan(\nu)\tan(\mu)}. \tag{D.3}$$

In order to derive equation (19) connecting the angles of the single RC circuits at any frequency to the mirror-symmetric point, we examine:

$$\begin{aligned} \tan(\tilde{\varphi}) &= \tan(\pi-\varphi) = -\tan(\varphi) \\ &= -\frac{(\omega R_+C_+)+(\omega R_-C_-)}{1-(\omega R_+C_+)(\omega R_-C_-)} \\ &= \frac{\frac{1}{(\omega R_-C_-)}+\frac{1}{(\omega R_+C_+)}}{1-\frac{1}{(\omega R_+C_+)}\frac{1}{(\omega R_-C_-)}} \\ &= \frac{\tan\left(\frac{\tilde{\varphi}_+}{2}\right)+\tan\left(\frac{\tilde{\varphi}_-}{2}\right)}{1-\tan\left(\frac{\tilde{\varphi}_+}{2}\right)\tan\left(\frac{\tilde{\varphi}_-}{2}\right)} = \tan\left(\frac{\tilde{\varphi}_++\tilde{\varphi}_-}{2}\right). \end{aligned} \tag{D.4}$$

Comparing the single terms leads to:

$$\begin{aligned}\tan\left(\frac{\tilde{\varphi}_{\pm}}{2}\right) &= \tilde{\omega}R_{\pm}C_{\pm} = \frac{1}{\omega R_{\mp}C_{\mp}}\\ &= \frac{1}{\tan\left(\frac{\varphi_{\mp}}{2}\right)} = -\tan\left(\frac{\pi}{2}+\frac{\varphi_{\mp}}{2}\right)\\ &= \tan\left(\pi-\left(\frac{\pi}{2}+\frac{\varphi_{\mp}}{2}\right)\right)\\ &= \tan\left(\frac{\pi}{2}-\frac{\varphi_{\mp}}{2}\right).\end{aligned} \tag{D.5}$$

Finally, we prove the mirror symmetry of two RC circuits with equal ohmic resistances and arbitrary capacitances,

$$\begin{aligned}Z_{2RC}(\varphi)+\overline{Z_{2RC}(\pi-\varphi)} &= Z_{2\,\mathrm{RC}}(\varphi_+,\varphi_-)+\overline{Z_{2\,\mathrm{RC}}(\tilde{\varphi}_+,\tilde{\varphi}_-)} = Z_{2\,\mathrm{RC}}(\varphi_+,\varphi_-)+\overline{Z_{2\,\mathrm{RC}}(\pi-\varphi_-,\pi-\varphi_+)}\\ &= \frac{R}{2}\left(1+\cos\left(\frac{\varphi_+-\varphi_-}{2}\right)\cdot \mathrm{e}^{-\mathrm{i}\frac{\varphi_++\varphi_-}{2}}\right)+\frac{R}{2}\left(1+\cos\left(\frac{\varphi_+-\varphi_-}{2}\right)\cdot \mathrm{e}^{i\pi}\mathrm{e}^{-\mathrm{i}\frac{\varphi_++\varphi_-}{2}}\right)\\ &= \frac{R}{2}\left(1+\cos\left(\frac{\varphi_+-\varphi_-}{2}\right)\cdot \mathrm{e}^{-\mathrm{i}\frac{\varphi_++\varphi_-}{2}}\right)+\frac{R}{2}\left(1-\cos\left(\frac{\varphi_+-\varphi_-}{2}\right)\cdot \mathrm{e}^{-\mathrm{i}\frac{\varphi_++\varphi_-}{2}}\right)=R.\end{aligned} \tag{D.6}$$

Moreover, (26) follows from:

$$\begin{aligned}Z_{2RC}(\omega) &= \frac{R_+}{1+\mathrm{i}\omega R_+C_+}+\frac{R_-}{1+\mathrm{i}\omega R_-C_-} = \frac{R_+}{1+(\omega R_+C_+)^2}+\frac{R_-}{1+(\omega R_-C_-)^2}+\mathrm{i}\left(\frac{-R_+(\omega R_+C_+)}{1+(\omega R_+C_+)^2}+\frac{-R_-(\omega R_-C_-)}{1+(\omega R_-C_-)^2}\right)\\ &= \frac{R_++R_-+R_+(\omega R_-C_-)^2+R_-(\omega R_+C_+)^2}{1+(\omega R_+C_+)^2+(\omega R_-C_-)^2+(\omega R_+C_+)^2(\omega R_-C_-)^2}\\ &\quad+\mathrm{i}\frac{-R_+(\omega R_+C_+)-R_-(\omega R_-C_-)-(\omega R_+C_+)(\omega R_-C_-)(R_+(\omega R_-C_-)+R_-(\omega R_+C_+))}{1+(\omega R_+C_+)^2+(\omega R_-C_-)^2+(\omega R_+C_+)^2(\omega R_-C_-)^2}\\ &= \frac{R+\frac{R}{2}(\omega RC)^2\left(\tan^2\left(\frac{\pi}{4}+\frac{\beta}{2}\right)+\tan^2\left(\frac{\pi}{4}-\frac{\beta}{2}\right)\right)}{1+2\,(\omega RC)^2\left(\tan^2\left(\frac{\pi}{4}+\frac{\beta}{2}\right)+\tan^2\left(\frac{\pi}{4}-\frac{\beta}{2}\right)\right)+(\omega RC)^4\left(\tan\left(\frac{\pi}{4}+\frac{\beta}{2}\right)\tan\left(\frac{\pi}{4}-\frac{\beta}{2}\right)\right)^2}\\ &\quad+\mathrm{i}\frac{-\frac{R}{2}(\omega RC)\left(\tan\left(\frac{\pi}{4}+\frac{\beta}{2}\right)+\tan\left(\frac{\pi}{4}-\frac{\beta}{2}\right)\right)-\frac{R}{2}(\omega RC)^3\left(\tan\left(\frac{\pi}{4}+\frac{\beta}{2}\right)\tan\left(\frac{\pi}{4}-\frac{\beta}{2}\right)\right)\left(\tan\left(\frac{\pi}{4}+\frac{\beta}{2}\right)+\tan\left(\frac{\pi}{4}-\frac{\beta}{2}\right)\right)}{1+2\,(\omega RC)^2\left(\tan^2\left(\frac{\pi}{4}+\frac{\beta}{2}\right)+\tan^2\left(\frac{\pi}{4}-\frac{\beta}{2}\right)\right)+(\omega RC)^4\left(\tan\left(\frac{\pi}{4}+\frac{\beta}{2}\right)\tan\left(\frac{\pi}{4}-\frac{\beta}{2}\right)\right)^2}\\ &= \frac{R+R(\omega RC)^2\frac{1+\sin^2(\beta)}{\cos^2(\beta)}}{1+2\,(\omega RC)^2\frac{1+\sin^2(\beta)}{\cos^2(\beta)}+(\omega RC)^4}+\mathrm{i}\frac{-\frac{R}{\cos(\beta)}(\omega RC)-\frac{R}{\cos(\beta)}(\omega RC)^3}{1+2\,(\omega RC)^2\frac{1+\sin^2(\beta)}{\cos^2(\beta)}+(\omega RC)^4}\\ &= \frac{R\cos^2(\beta)+R(\omega RC)^2\left(1+\sin^2(\beta)\right)}{\cos^2(\beta)\left(1+(\omega RC)^4\right)+2\,(\omega RC)^2\left(1+\sin^2(\beta)\right)}+\mathrm{i}\frac{-R\cos(\beta)(\omega RC)\left(1+(\omega RC)^2\right)}{\cos^2(\beta)\left(1+(\omega RC)^4\right)+2\,(\omega RC)^2\left(1+\sin^2(\beta)\right)}\\ &= \frac{R\cos^2(\beta)\left(1-(\omega RC)^2\right)+2\,R(\omega RC)^2}{\cos^2(\beta)\left(1-(\omega RC)^2\right)^2+4\,(\omega RC)^2}+\mathrm{i}\frac{-R\cos(\beta)(\omega RC)\left(1+(\omega RC)^2\right)}{\cos^2(\beta)\left(1-(\omega RC)^2\right)^2+4\,(\omega RC)^2}.\end{aligned} \tag{D.7}$$

Consequently, equality (27) is:

$$\begin{aligned}\tan(\varphi) &= \frac{-\mathrm{Im}\left[Z_{2RC}(\omega)\right]}{\mathrm{Re}\left[Z(\omega)\right]-\frac{R}{2}}\\ &= \frac{(\omega R_+C_+)+(\omega R_-C_-)}{1-(\omega R_+C_+)(\omega R_-C_-)}\\ &= \frac{\left(\omega RC\tan\left(\frac{\pi}{4}+\frac{\beta}{2}\right)\right)+\left(\omega RC\tan\left(\frac{\pi}{4}-\frac{\beta}{2}\right)\right)}{1-\left(\omega RC\tan\left(\frac{\pi}{4}+\frac{\beta}{2}\right)\right)\left(\omega RC\tan\left(\frac{\pi}{4}-\frac{\beta}{2}\right)\right)}\\ &= \frac{2\,\omega RC}{\left(1-(\omega RC)^2\right)}\frac{1}{\cos(\beta)},\end{aligned} \tag{D.8}$$

with

$$\tan\left(\frac{\pi}{4}+\frac{\beta}{2}\right)\tan\left(\frac{\pi}{4}-\frac{\beta}{2}\right)=1 \tag{D.9}$$

$$\tan^2\left(\frac{\pi}{4}+\frac{\beta}{2}\right)+\tan^2\left(\frac{\pi}{4}-\frac{\beta}{2}\right)=2\,\frac{1+\sin^2(\beta)}{\cos^2(\beta)} \tag{D.10}$$

$$\tan\left(\frac{\pi}{4}+\frac{\beta}{2}\right)+\tan\left(\frac{\pi}{4}-\frac{\beta}{2}\right)=\frac{2}{\cos(\beta)}. \tag{D.11}$$

Appendix E. Computation in detail: ZAPP

The computation of ZAPP is also split into a real part and an imaginary part. We start with the real part (35):

$$\begin{aligned}
\mathrm{Re}\left[Z_{\mathrm{APP}}(\omega)\right] &= \lim_{N\to\infty}\mathrm{Re}\left[Z_N(\omega)\right] = \frac{R}{\beta}\int_{\frac{\pi}{4}-\frac{\beta}{2}}^{\frac{\pi}{4}+\frac{\beta}{2}}\frac{1}{1+(\omega RC)^2\tan^2(x)}\mathrm{d}x = \frac{R}{\beta}\int_{\frac{\pi}{4}-\frac{\beta}{2}}^{\frac{\pi}{4}+\frac{\beta}{2}}\frac{\cos^2(x)}{\cos^2(x)+(\omega RC)^2\sin^2(x)}\mathrm{d}x\\
&= \frac{R}{\beta}\left[\frac{x}{1-(\omega RC)^2}-\frac{(\omega RC)}{1-(\omega RC)^2}\arctan\left((\omega RC)\tan(x)\right)\right]_{\frac{\pi}{4}-\frac{\beta}{2}}^{\frac{\pi}{4}+\frac{\beta}{2}}\\
&= R\left(\frac{1}{1-(\omega RC)^2}-\frac{(\omega RC)}{\left(1-(\omega RC)^2\right)\beta}\left(\arctan\left((\omega RC)\tan\left(\frac{\pi}{4}+\frac{\beta}{2}\right)\right)-\arctan\left((\omega RC)\tan\left(\frac{\pi}{4}-\frac{\beta}{2}\right)\right)\right)\right)\\
&= R\left(\frac{1}{1-(\omega RC)^2}-\frac{(\omega RC)}{\left(1-(\omega RC)^2\right)\beta}\arctan\left(\frac{(\omega RC)\tan\left(\frac{\pi}{4}+\frac{\beta}{2}\right)-(\omega RC)\tan\left(\frac{\pi}{4}-\frac{\beta}{2}\right)}{1+(\omega RC)^2\tan\left(\frac{\pi}{4}+\frac{\beta}{2}\right)\tan\left(\frac{\pi}{4}-\frac{\beta}{2}\right)}\right)\right)\\
&= \frac{R}{2}\left(1+\frac{1+(\omega RC)^2}{1-(\omega RC)^2}-\frac{2\ (\omega RC)}{\left(1-(\omega RC)^2\right)\beta}\arctan\left(\frac{2\ (\omega RC)}{\left(1+(\omega RC)^2\right)}\tan(\beta)\right)\right),
\end{aligned} \tag{E.1}$$

where we used,

$$\arctan(x)-\arctan(y)=\arctan\left(\frac{x-y}{1+xy}\right) \tag{E.2}$$

$$\tan(x)\pm\tan(y)=\frac{\sin(x\pm y)}{\cos(x)\cos(y)} \tag{E.3}$$

$$\frac{\tan(x)-\tan(y)}{1+c\tan(x)\tan(y)}=\frac{2\sin(x-y)}{(1+c)\cos(x-y)+(1-c)\cos(x+y)}. \tag{E.4}$$

In order to compute (36), we need the following:

$$\cos^2(x)=\frac{1}{2}\left(1+\cos(2x)\right) \tag{E.5}$$

$$\sin^2(x)=\frac{1}{2}\left(1-\cos(2x)\right) \tag{E.6}$$

$$\operatorname{artanh}(x)=\frac{1}{2}\ln\left(\frac{1+x}{1-x}\right)\ \text{for}\ |x|<1, \tag{E.7}$$

and finally, we compute the imaginary part of ZAPP:

$$\begin{aligned}
\mathrm{Im}\left[Z_{\mathrm{APP}}(\omega)\right] &= \lim_{N\to\infty}\mathrm{Im}\left[Z_N(\omega)\right]\\
&= -\frac{R}{\beta}\int_{\frac{\pi}{4}-\frac{\beta}{2}}^{\frac{\pi}{4}+\frac{\beta}{2}}\frac{(\omega RC)\tan(x)}{1+(\omega RC)^2\tan^2(x)}\mathrm{d}x\\
&= -\frac{R}{2\,\beta}\int_{\frac{\pi}{4}-\frac{\beta}{2}}^{\frac{\pi}{4}+\frac{\beta}{2}}\frac{2\ (\omega RC)\sin(x)\cos(x)}{\cos^2(x)+(\omega RC)^2\sin^2(x)}\mathrm{d}x\\
&= -\frac{R}{2\,\beta}\left[-\frac{(\omega RC)}{\left(1-(\omega RC)^2\right)}\right.\\
&\qquad\left.\times\ln\left(\cos^2(x)+(\omega RC)^2\sin^2(x)\right)\right]_{\frac{\pi}{4}-\frac{\beta}{2}}^{\frac{\pi}{4}+\frac{\beta}{2}}\\
&= -\frac{R}{2}\,\frac{(\omega RC)}{\left(1-(\omega RC)^2\right)\beta}\\
&\qquad\times\ln\left(\frac{\left(1+(\omega RC)^2\right)+\sin(\beta)\left(1-(\omega RC)^2\right)}{\left(1+(\omega RC)^2\right)-\sin(\beta)\left(1-(\omega RC)^2\right)}\right)
\end{aligned}$$

$$= -\frac{R}{2}\frac{2\,(\omega RC)}{\left(1-(\omega RC)^2\right)\beta} \times \operatorname{artanh}\left(\frac{1-(\omega RC)^2}{1+(\omega RC)^2}\sin(\beta)\right). \tag{E.8}$$

Appendix F. Computation in detail: three RC circuits

The computation of the total capacitance of three serial connected RC circuits (55) is as follows:

$$\begin{aligned}\frac{C}{C_{\mathrm{tot,3RC}}} &= \frac{C}{C_1}+\frac{C}{C_{2+}}+\frac{C}{C_{2-}}\\ &= \frac{\tan\left(\frac{\alpha}{4}\pi\right)-\sin\left(\frac{\pi}{2}-\xi\right)}{1-\sin\left(\frac{\pi}{2}-\xi\right)}+\frac{1-\tan\left(\frac{\alpha}{4}\pi\right)}{2\,\tan\left(\frac{\pi}{4}+\frac{\xi}{2}\right)\left(1-\sin\left(\frac{\pi}{2}-\xi\right)\right)}+\frac{1-\tan\left(\frac{\alpha}{4}\pi\right)}{2\,\tan\left(\frac{\pi}{4}+\frac{\xi}{2}\right)\left(1-\sin\left(\frac{\pi}{2}-\xi\right)\right)}\\ &= \frac{1}{1-\sin\left(\frac{\pi}{2}-\xi\right)}\left(\tan\left(\frac{\alpha}{4}\pi\right)-\sin\left(\frac{\pi}{2}-\xi\right)+\frac{1-\tan\left(\frac{\alpha}{4}\pi\right)}{2}\left(\frac{1}{\tan\left(\frac{\pi}{4}+\frac{\xi}{2}\right)}+\tan\left(\frac{\pi}{4}+\frac{\xi}{2}\right)\right)\right)\\ &= \frac{1}{1-\sin\left(\frac{\pi}{2}-\xi\right)}\left(\tan\left(\frac{\alpha}{4}\pi\right)-\sin\left(\frac{\pi}{2}-\xi\right)+\frac{1-\tan\left(\frac{\alpha}{4}\pi\right)}{\sin\left(\frac{\pi}{2}+\xi\right)}\right)\\ &= 1+\frac{1-\tan\left(\frac{\alpha}{4}\pi\right)}{\sin\left(\frac{\pi}{2}-\xi\right)}.\end{aligned} \tag{F.1}$$

ORCID iDs

Thomas Heil https://orcid.org/0000-0003-1997-8781
Andreas Jossen https://orcid.org/0000-0003-0964-1405

References

[1] Debye P 1929 Polar molecules *Chem. Catalog Company* **48** 1036–7
[2] Cole K and Cole R 1941 Dispersion and absorption in dielectrics *J. Chem. Phys.* **9** 341–51
[3] Jonscher A 1974 Hopping losses in polarisable dielectric media *Nature* **250** 191–3
[4] Fricke H 1932 XXXIII. The theory of electrolytic polarization *Lond. Edinburgh Dublin Phil. Mag. J. Sci.* **14** 310–8
[5] Randles J 1947 Kinetics of rapid electrode reactions *Discuss. Faraday Soc.* **1** 11–9
[6] Brug G, Van Den Eeden A, Sluyters-Rehbach M and Sluyters J 1984 The analysis of electrode impedances complicated by the presence of a constant phase element *J. Electroanal. Chem.* **176** 275–95
[7] Jorcin J B, Orazem M, Pébère N and Tribollet B 2006 CPE analysis by local electrochemical impedance spectroscopy *Electrochim. Acta* **51** 1473–9
[8] Janshoff A, Wegener J, Steinem C, Sieber M and Galla H-J 1996 Applications of impedance spectroscopy in biochemistry and biophysics *Acta Biochim. Pol.* **43** 339–48
[9] Randviir E P and Banks C E 2013 Electrochemical impedance spectroscopy: an overview of bioanalytical applications *Anal. Methods* **5** 1098–115
[10] Grossi M and Riccò B 2017 Electrical impedance spectroscopy (EIS) for biological analysis and food characterization: a review *J. Sens. Sens. Syst.* **6** 303–25
[11] Dominguez-Benetton X, Sevda S, Vanbroekhoven K and Pant D 2012 The accurate use of impedance analysis for the study of microbial electrochemical systems *Chem. Soc. Rev.* **41** 7228–46
[12] Knudsen K B, Vegge T, McCloskey B D and Hjelm J 2016 An electrochemical impedance spectroscopy study on the effects of the surface- and solution-based mechanisms in Li-O2 cells *J. Electrochem. Soc.* **163** A2065
[13] Córdoba-Torres P, Mesquita T J and Nogueira R P 2015 Relationship between the origin of constant-phase element behavior in electrochemical impedance spectroscopy and electrode surface structure *J. Phys. Chem.* C **119** 4136–47
[14] Elwakil A S 2010 Fractional-order circuits and systems: an emerging interdisciplinary research area *IEEE Circuits Syst. Mag.* **10** 40–50
[15] Lukács Z and Kristóf T 2020 A generalized model of the equivalent circuits in the electrochemical impedance spectroscopy *Electrochim. Acta* **363** 137199
[16] Valsa J, Dvorak P and Friedl M 2011 Network model of the CPE *Radioengineering* **20** 619–26
[17] Krishna B T and Reddy K V V S 2008 Active and passive realization of fractance device of order 1/2 *Act. Passiv. Electron. Compon.* **2008** 1–5
[18] Machado J A 2001 Discrete-time fractional-order controllers *Fract. Calc. Appl. Anal.* **4** 47–66
[19] Buller S, Thele M, De Doncker R W and Karden E 2005 Impedance-based simulation models of supercapacitors and Li-ion batteries for power electronic applications *IEEE Trans. Ind. Appl.* **41** 742–7
[20] Buller S 2003Impedance based simulation models for energy storage devices in advanced automotive power systems PhD Thesis, RWTH Aachen, Aachen, Germany
[21] Farmann A, Waag W and Sauer D U 2015 Adaptive approach for on-board impedance parameters and voltage estimation of lithium-ion batteries in electric vehicles *J. Power Sources* **299** 176–88

[22] Handschuh T 2007 Untersuchung des Betriebs- und Alterungsverhaltens von Blei-Säure-Akkumulatoren bei für Hybridantriebssysteme typischen Belastungen PhD Thesis Ulm University, Ulm, Germany
[23] Lu L, Han X, Li J, Hua J and Ouyang M 2013 A review on the key issues for lithium-ion battery management in electric vehicles *J. Power Sources* **226** 272–88
[24] Plett G 2004 Extended kalman filtering for battery management systems of LiPB-based HEV battery packs: part 1. Background *J. Power Sources* **134** 252–61
[25] Plett G 2004 Extended kalman filtering for battery management systems of LiPB-based HEV battery packs: part 2. Modeling and identification *J. Power Sources* **134** 262–76
[26] Plett G 2004 Extended kalman filtering for battery management systems of LiPB-based HEV battery packs: part 3. State and parameter estimation *J. Power Sources* **134** 277–92
[27] Mittag-Leffler G M 1903 Sur la nouvelle fonction $e_{\alpha}(x)$ *C. R. Acad. Sci.* **137** 554–8
[28] Macdonald D and Urquidi-Macdonald M 1985 Application of Kramers–Kronig transforms in the analysis of electrochemical systems: I. Polarization resistance *J. Electrochem. Soc.* **132** 2316–9
[29] Urquidi-Macdonald M, Real S and Macdonald D 1986 Application of kramers-kronig transforms in the analysis of electrochemical impedance data: II. Transformations in the complex plane *J. Electrochem. Soc.* **133** 2018–24
[30] Urquidi-Macdonald M, Real S and Macdonald D 1990 Applications of Kramers–Kronig transforms in the analysis of electrochemical impedance data: III. Stability and linearity *Electrochim. Acta* **35** 1559–66
[31] Macdonald D and Urquidi-Macdonald M 1990 Kramers–Kronig transformation of constant phase impedances *J. Electrochem. Soc.* **137** 515–7
[32] Heaviside O 2011 *Electrical Papers* vol I 1st edn (Cambridge: CUP)
[33] Heaviside O 2011 *Electrical Papers* vol II 1st edn (Cambridge: CUP)
[34] Monje C A, Chen Y Q, Vinagre B M, Xue D and Feliu-Batlle V 2010 *Fractional-Order Systems and Controls: Fundamentals and Applications* (New York: Springer Science & Business Media)
[35] Garrappa R, Mainardi F and Guido M 2016 Models of dielectric relaxation based on completely monotone functions *Fract. Calc. Appl. Anal.* **19** 1105–60
[36] Berberan-Santos M N 2005 Properties of the Mittag–Leffler relaxation function *J. Math. Chem.* **38** 629–35
[37] De Oliveira E C, Mainardi F and Vaz J 2011 Models based on Mittag–Leffler functions for anomalous relaxation in dielectrics *Eur. Phys. J. Spec. Top.* **193** 161–71
[38] Gómez J F, Torres L and Escobar R F 2019 Studies in Systems, Decision and Control *Fractional Derivatives With Mittag–Leffler Kernel: Trends and Applications in Science and Engineering* (New York: Springer)
[39] Gröbner W and Hofreiter N 1975 *Integraltafel: Erster Teil: Unbestimmte Integrale* 5th edn (New York: Springer)
[40] Schuster S, Brand M, Berg P, Gleissenberger M and Jossen A 2015 Lithium-ion cell-to-cell variation during battery electric vehicle operation *J. Power Sources* **297** 242–51
[41] Illig J, Ender M, Chrobak T, Schmidt J P, Klotz D and Ivers-Tiffée E 2012 Separation of charge transfer and contact resistance in lifepo4-cathodes by impedance modeling *J. Electrochem. Soc.* **159** A952